Article:
Boushehri, K, Tsavdaridis, K orcid.org/0000-0001-8349-3979 and Cai, G (2019) Seismic Behaviour of RWS Moment Connections to Deep Columns with European Sections. Journal of Constructional Steel Research, 161. pp. 416-435. ISSN 0143-974X

https://doi.org/10.1016/j.jcsr.2019.07.009

Seismic Behaviour of RWS Moment Connections to Deep Columns with European Sections

[1]Kavoos Boushehri, [*2]Konstantinos Daniel Tsavdaridis and [3]Gaochuang Cai

[1]Research Assistant, School of Civil Engineering, University of Leeds, Woodhouse Lane, LS2 9JT, Leeds

[2]Associate Professor of Structural Engineering, School of Civil Engineering, University of Leeds, Woodhouse Lane, LS2 9JT, Leeds

[3]Assistant Professor, Faculty of Engineering, Fukuoka University, Fukuoka, 184-0180, Japan

[*]*Corresponding Author (k.tsavdaridis@leeds.ac.uk)*

ABSTRACT

The design of reduced web section (RWS) connections is becoming more often, while the research is focusing on both areas: (a) the performance of beams with large web opening areas near the supports, and (b) the seismic behaviours of steel beam-to-column connections of different types when subjected to cyclic loads. The beam web opening is used as a mechanism to counterbalance the low inelastic capacity of the welds and to shift the stresses from the welding and shear panel zones to the weak beam section in line with the concept of "weak beam-strong column" often employed for the seismic-resistant design of Moment Resisting Frames (MRFs). However, limited data yet exists on the design and seismic behaviour of such connections and those are only for UKB and UKC section profiles. This paper presents an extensive FE study of the seismic performance of fully welded RWS moment connections to deep columns. The effect of using different beam spans is also investigated together with the effect of web opening size and position (web opening at different shear-moment interactions). European HE and IPE profiles are employed for this study in an effort to introduce RWS connections in Eurocode 8, and understand potential variations in design when using European sections as previously reported in RBS connections. Finally, a design procedure is thoroughly presented based on AISC 358 (AISC 358, 2010).

Keywords: RWS connections; seismic-resistant MRFs; perforated beams; Vierendeel mechanism; local bucking; fully welded connections

1. Introduction

Steel moment resisting frames (MRFs) with rigid connections between beams and columns have been widely used because of their lateral load resistance and good seismic behaviour. In the 1994 Northridge earthquake, fragile cracks were found in beam-column connections due to the inelastic behaviour of either Complete Joint Penetration (CJP), Partial Joint Penetration (PJP), or fillet welds between the beams and the columns. Many different buildings have been investigated, in which it was suggested that all these fractures were unanticipated and the beam-column connections were not well understood (FEMA 350, 2000). Solutions were since considered by reinforcing connections or having a Reduced Beam Section (RBS) type of connection as shown in **Figure 1** (FEMA 350, 2000; AISC 358, 2010; EC8 Part 3, 2005;). in order to achieve the "*weak beam-strong column*" mechanism which eventually shifts the plastic hinge to be formed in the beam.

There is vast numerical and experimental research on RBS connections; a few relavant to this research findings are reported herein. For example, Uang et al. (2000) concluded that the brittle fracture of the welds found in pre-Northridge connection can be improved by replacing the low-toughness welds with a notch-toughness electrode. Uang et al. (2000b) observed that all specimens can reach over 0.03rad of rotation and specimens with near-fault loading protocol can reach 0.05rad while the majority of the dissipated energy occurs at the RBS weakened region. Wang et al. (2008) studied RBS connected to Concrete Filled Steel Tubular (CFST) columns, which in case of strong panel zone and adequate column connection strength, exhibited well seismic performance. Li et al. (2019) studied RBS connections with H-section beams and it was found that in this case the values of a, b and c as proposed by AISC 358 (2010) should be amended. This demonstrated that when beam section other than the American ones, may yield different behaviours because of their different thickness and height aspect ratios.

More recently, the concept of 'merging' the purposely weakened connections with the use of perforated beams was investigated, as a trend of achieving material efficiency and considering material reduction through beam web cuts, also known as Reduced Web Section (RWS). On the other hand, the local shear capacity (because of shear plastic hinges) of the beams is decreased because of the opening existence, thus the moment capacity is decreased, which yields an increase in the rotational capacity. It was initially proven that RWS connections provide a higher rotational capacity of the order of 0.05rad, and Hedayat, M. Celikag (2009) recommends a minimum of 0.04rad, whilst 0.035rad is suggested by FEMA 350 (2000) and EC8 Part 3 (2005) to be acceptable in seismic design. Thereafter, limited research was conducted regarding the design limitations of such connections when perforated beams with standard and non-standard isolated web openings are used (Tsavdaridis et al., 2014 and 2017), as well as when fully perforated (aka cellular beams) are employed (Tsavdaridis and Papadopoulos, 2016). Later, research on composite RWS connections was conducted (Shaheen et al., 2018).

Tsavdaridis et al. (2014) studied welded perforated steel beam-to-column connections subjected to cyclic loading. The SAC (2000) loading protocol was used to load the specimens, and several nonlinear finite element (FE) studies were undertaken to understand the behaviour of the connections when compared with an RBS connection and a connection using a solid beam. The results showed that the presence of a web opening resulted in a reduction in moment capacity and rotational stiffness, as expected. The opening depth, d_0, has the highest impact on the connection's strength and the end

distance from column face, *S*, also has a notable impact on both moment capacity and behaviour of the connections. Erfrani and Akrami (2017) investigated the energy dissipation when using RWS connections. Different opening sizes and lengths were studied. It was found that the minimum drift at which the fracture happened at the opening corner was at 4%. Openings closer to the column face showed a better effect on the connection behaviour. It was concluded that an appropriate size and location of the perforation can effectively increase the energy dissipation and ductility of the connection. Moreover, Momenzadeh, et al. (2017) also studied the behaviour of RWS connections and found that these connections can mobilise the plastic hinges away from the column face near the location of the perforation. Specific geometric characteristics for RWS connections were also suggested to attain the desired behavior. Naughton et al. (2017) performed pushover analyses on a number of MRFs using RBS, RWS, and solid beam connections. The research demonstrated the effectiveness of RWS connections which results in the "weak beam-strong column" mechanism for the entire frame. Ultimately, Shaheen et al. (2018) studied RWS composite beam-to-column connection behaviours and compared them against the non-composite connections. It was concluded that the composite action reduces the ductility of the connection. Opening size and distance to column face controls the performance of the connection. Concrete crushing at face of the column in conventional connections, appears in the vicinity of the web opening in RWS connections. As the opening size increases the composite action contribution to load bearing increases.

Overall, the position, size, and web opening configuration can lead to an efficient method of improving the aseismic behaviour by controlling the inelasticity of the beams with regards to that of the welds found in moment connections. Other research studies are quoting similar results (Tsavdaridis et al., 2017; Naughton et al., 2017).

The above studies on RBS connections recommend that further research is required to understand how all geometric parameters can affect the performance of RWS connections, and what to optimise in order to achieve a controlled behaviour. Furthermore, it was concluded that the standard design guidelines for RBS connections are note adequate for RWS connections and that modifications are necessary. Consequently, this paper examines the behaviour of RWS beam-column connections under cyclic loading scoping to introduce them as prequalified connections for special and intermediate steel moment frames for seismic applications to the European Codes of Practice - Eurocode 8 (and to AISC 358) in the future following large experimental and computational studies.

2. Methodology

A range of European IPE beams and HE columns, opening sizes (small, medium and large), and opening positions (shear-moment interactions vary) are examined herein; factors that affect the connection's load carrying and rotational capacities, energy dissipation capabilities, and inter-story drifts.

In detail, stress distribution patterns in the vicinity of the web openings are examined investigating the effect of the position of the web openings with distances from column face depending on the beam height (h), one at 0.87h, one at 1.3h and one at 1.74h. To examine the effect of the size of the web openings, this parametric study considers three different web opening sizes, with a diameter depending on the beam height (h), equal to 0.50h, 0.65h, and 0.80h. To examine the effect of beam size, this parametric study will consider four different beam sizes, IPE300, IPE450, IPE500 and

IPE600 with corresponding column sizes and other joint components such as stiffeners, continuity plates, and doubler web plates. To examine the effect of different spans, this parametric study considers four different spans to keep the span/depth above a threshold (AISC 358, 2010) , thus two sets of spans were considered equal to 3m, 5m, 10m and 15m and 5m, 10m, 15m and 20m (for higher depth beams). To investigate all the parameters (i.e., 4 x spans, 4 x column sizes, 3 x opening sizes, and 3 x opening end distances from the face of the column), 144 models in addition to the 4 models with solid webbed beams, a total of 148 models (data points) is required. Due to CPU limitations, cyclic analyses are computationally expensive, 52 models were created and the rest of the results were produced through linear interpolation.

3. Finite element model validation

3.1. Model

An FE model of an RBS connection was initially modelled using ABAQUS 6.14 (ABAQUS, 2014) and, was validated against Pachoumis et al. (2009) experimental test (**Figure 2**). Similar to what was presented in previous research papers on RWS connections, an RBS connection was utilised for the validation study due to lack of experimental works which provide enough information on RWS connections. It is, however, considered following some preliminary studies, that the RBS geometric configuration will not impact the accuracy of the analyses modelling. Yet, the possibility of obtaining different strength degradation between RBS and RWS connections is apparent. Specimen RBS1 in Pachoumis et al. (2009) was chosen for the validation as a full plastic hinge formation was demonstrated. The beam-to-column connection model includes high-quality welds at the face of the column, doubler web plates, and continuity plates, with the thickness chosen to be equal to the beam flange thickness so that they can produce a strong panel zone, forcing the formation of the plastic hinge in the RBS zone. The beam, column, doubler plates, and continuity plates' dimensions are summarised in **Table 1**. The RBS connections were designed according to the recommendations proposed by EC8 Part 3 (2005), resulting in dimensions for the RBS region are noted in **Table 2**.

Table 1. Test set-up dimensions (Pachoumis et al., 2009).

Section		$W_{pl,y}$ cm^3	h mm	b mm	t_w mm	t_f mm	Doubler Plate			Continuity Plate		
							h	b	t	h	b	t
Beam	HE 240A	745	230	240	7.5	12.0	460	208	12.0	262	116	10.0
Column	HE 300 B	1869	300	300	11.0	19.0						

$W_{pl,y}$ Plastic section modulus

Table 2. The details of RBS Region in specimen RBS1.

b_f mm	d_b mm	a mm	b mm	s mm	c mm	r mm

240	230	156	184	248	60	100.53

As shown in Figure 2,

a	Distance of the beginning of the RBS from the column face.
b	Length of the RBS
c	Radius of the RBS cut
r	Radius of circular web opening

3.2. Modelling assumptions

Since the ultimate strain (ε) was not presented in the literature (Pachoumis et al., 2009), a series of different strain ratios were tested to examine which one yields better results. When ε=0.15 was used, higher moments than the one found in the literature were yielded while when ε=0.25, the results were much lower. Hence, ε=0.205 was chosen with a corresponding tangent modulus, E_t=1000 N/mm^2. Other researchers that validated their model against this experimental study also used this ultimate strain (Tsavdaridis, et al., 2014) and experimental observations of Tsavdaridis and D'Mello (2011). According to Tsavdaridis et al. (2014), none of the welds were modelled for the ease of analysis while full continuity was applied. Column supports were modelled as fixed at both ends in all directions not allowing rotation and translation in any direction. The beam end was fixed against the out-of-plane translation in distances of 1.5m while simulating the presence of side beams to prevent lateral torsional buckling. The same assumptions as they one in the literature were followed to better establish the comparisons and make possible conclusions.

3.3. Material properties

Nonlinear material properties were used for all sections of the steel frame, with Young's modulus E=207,000 N/mm^2, yield stress f_y=305 N/mm^2 and ultimate stress f_u=510 N/mm^2 as shown in **Figure 3**. The four- node shell element (S4R in ABAQUS) with reduced integration (Nascimbene, 2014) was used, and finer mesh applied to critical areas of the subassemblies like RBS region. ε=0.205 was chosen with a corresponding tangent modulus, E_t=1000 N/mm^2. The density of the material (7850kg/m^3) was also introduced as the weight may also affect the moment capacity of the connection. **Figure 3** shows the constitutive model of the material.

3.4. Loading and analysis

A displacement-control type of reversed cyclic loading was used based on the SAC loading Protocol (FEMA 350, 2000) as shown in **Figure 4**, while the displacement was calculated based on the peak deformation corresponding to the load step number.

Beam end displacement calculations are tabulated in **Table 3**. The analysis was conducted by applying cyclic variable amplitude displacement at the top of the beam in a distance of 1.00 m from the face of the column. A number of simplifications were made while designing this connection: the welds were not modelled, and the root radius of the beam and column were not modelled. A nonlinear full Newton–Raphson direct method was used for the analysis. Increment size for sub-steps was set to automatic to be controlled by the program to decrease it when needed to achieve convergence and avoid getting analysis errors.

Table 3. RBS beam end displacement.

Load Step			1	2	3	4	5	6	7	8	9
Cycle Number			1-6	6-12	12-18	18-22	22-24	24-26	26-28	28-30	30-32
Peak Rotation ϕ			0.00375	0.005	0.0075	0.01	0.015	0.02	0.03	0.04	0.05
Span m	**h_c** m	**L_{CL}** m	**Beam end displacements** (mm) $\Delta L_{CL}=\phi*L_{CL}$								
2	0.30	1.15	4.31	5.75	8.63	11.50	17.25	23.00	34.50	46.00	57.50

h_b Overall height of steel beam
h_c Overall height of steel column
LCL Distance from beam end to column centreline

3.5. Results of FE model

The moment-rotation hysteretic responses of the beam obtained by FE analyses are compared with those of the experimental study of Pachoumis et al. (2009) in order to verify the validity of the numerical model.

In the experimental work, moment-rotation curves were obtained for three different distances from the column face: (i) at 4 cm, (ii) at the RBS centreline, and (iii) at 75 cm away from the column face. All bending moments are computed as M=P*L, where L is the distance between the load axis and the column face axis (1.00 m) and P is the load. Rotations are calculated by dividing the deflection (displacement) by the distance from the column face (i.e., 4cm and 75cm).

Figure 5 depicts the comparison between the experimental and FE models conducted in the literature (Pachoumis et al., 2009) together with the new FE study carried out in this paper and it projects a satisfactory validation. Several parameters, such as tangent modulus, mesh size, loading point of along the beam end, beam end displacement amplitude, with or without end-plate, with or without sideways end restraint were changed in order to investigate their effect on the hysteresis behaviour and achieve a better calibration, however no one of these changes resulted in any favourable result. Some minor difference might be due to factors, such as the lack of information on the material's inelastic properties, residual stresses, experimental uncertainties, imperfections existing in the experimental samples, boundary conditions, and/or human errors.

4. Parametric study

4.1. Test set-ups

The parametric study involves a beam-to-column connection with singular circular beam web opening sections, known as reduced web sections (RWS), subjected to cyclic loading. Four different test setups are prepared with different beam and column sizes, different spans, different opening sizes, and distance. It is worth to note that this is the first study ever done on RWS connections using European profiles, while the vast majority of previous researches has been done on Universal Beams (UB) and Columns (UC) sections, thus the applicability of previously made observations is also under question. Pachoumis, et al. (2009) concluded that RBS connections designed to EC8 parameters which are derived from AISC (AISC 358, 2010) resulted in a poor seismic performance. Sophianopoulos and Deri (2017) also proposed that existing North-American and European recommendations for the design of RBS connections using European profiles may be optimised to satisfy all requirements of

the seismic design. Thus, simply using the American code's parameters for European sections is somewhat improper. In order to better observe and compare the results of the RWS connections, a connection with a solid (unperforated) beam for every test setup is also examined. As it was aforementioned, overall 52 FE models were examined in this paper. In order to choose the appropriate column size for each test setup, the plastic bending moment of every beam was calculated separately using EC3 (Eurocode 3, 2005) and then based on this moment the required plastic section modulus was obtained to find the column. In order to design for a strong panel zone, the column's required plastic section modulus has been calculated as twice the plastic moment capacity of the beam. Thus, the required plastic section modulus is calculated and tabulated in **Table 4**.

Table 4. Test set-ups required column section.

Test Set-up	**Beam Section**	**$W_{pl,y}$** (cm^3)	**$M_{c,Rd} = M_{pl,Rd} = W_{pl,y}*f_y/\gamma_{M0}$** (kNm)		**Column required $W_{pl,y}$** (cm^3)		**Column Section**	**$W_{pl,y}$** (cm^3)
A	HE 240A	745	745*305/1*10^-3 =	**227.2**	2*227.2*10^3*1/305 =	**1490**	HE 300 B	**1869**
B	IPE 330	804	804*305/1*10^-3 =	**245.2**	2*245.2*10^3*1/305 =	**1608**	HE 300 B	**1869**
C	IPE 450	1702	1702*305/1*10^-3 =	**519.1**	2*519.1*10^3*1/305 =	**3404**	HE 450 B	**3982**
D	IPE 500	2194	2194*305/1*10^-3 =	**669.2**	2*669.2*10^3*1/305 =	**4388**	HE 500 B	**4812**
E	IPE 600	3512	3512*305/1*10^-3 =	**1071.2**	2*1071.2*10^3*1/305 =	**7024**	HE 650 B	**7320**

4.2. Parameters

Test setup sections and subassemblies are tabulated in **Table 5**. Test setup A is the RBS1 connection, the same with the experimental test, while the other four setups are used to create the FE models for this parametric study. According to every setup, appropriate doubler web plates and continuity plates were used for the setup to result in a strong panel zone to reduce the inelastic demand of the column in comparison with the beam and welds. Continuity plate thickness is taken equal to beam's flange thickness and doubler plate thickness equal to the column's web thickness in all cases.

Table 5. The details of all studied test set-ups.

Test Setup	**Section**		**$W_{pl,y}$** cm^3	**h** mm	**b** mm	**t_w** mm	**t_f** mm	**Doubler Plate**			**Continuity Plate**		
								h	**b**	**t**	**h**	**b**	**t**
A	Beam	HE 240 A	745	230	240	7.5	12.0	460	208	12.0	262	116	10.0
	Column	HE 300 B	1869	300	300	11.0	19.0						
B	Beam	IPE 330	804	330	160	7.5	11.5	660	200	11.0	300	150	11.5
	Column	HE 300 B	1869	300	300	11.0	19.0						
C	Beam	IPE 450	1702	450	190	9.4	14.6	900	350	14.0	450	150	14.6
	Column	HE 450 B	3982	450	300	14.0	26.0						
D	Beam	IPE 500	2194	500	200	10.2	16.0	1000	400	14.5	500	150	16.0
	Column	HE 500 B	4812	500	300	14.5	38.0						
E	Beam	IPE 600	3512	600	220	12.0	19.0	1200	550	16.0	650	150	19.0
	Column	HE 650 B	7320	650	300	16.0	31.0						

For consistency, the same notations presented in previous research studies of RWS connections (Tsavdaridis et al., 2014), are employed. Three different values for each parameter (opening sizes d_0, and distances S) have been examined to investigate their effect on the moment capacity and behaviour, as be seen in **Figure 6**. **Table 6** includes all examined connection models and highlights the specimens

tested and used to interpolate to rest of the results. All results are presented for completeness and providing valuable information to practising engineers.

Where the clear span-to-depth ratio of beams in steel moment frames is less than 8, the qualifying total drift angle capacities shall be increased according to FEMA 350 (2000), which forces to satisfy higher rotation capacities: "*Where the clear-span-to-depth ratio of beams in the steel moment frame is less than 8, the qualifying total drift angle capacities indicated in Table 3-15 shall be increased to* q'_{SD} *and* q'_{U}*, given by equations 3-70 and 3-71, respectively.*", while ratios below 7 are not recommended for a seismic resistant connection. Therefore, in the setup D and E, the minimum span has changed from 3m to 5m so as to prevent an undesirable and non-compatible with FEMA 350 connection configuration with a very low span-to-depth ratio.

Table 6. Test specimens.

Test Setup	Span (m)	h (mm)	Span /h	S (mm)	Opening 1, d_0=0.50h			Opening 2, d_0=0.65h			Opening 3, d_0=0.80h		
					d_0	S_h	Setup	d_0	S_h	Setup	d_0	S_h	Setup
B	3	330	9.1	198	165	280.5	B1-198-3	215	305.25	B2-198-3	264	330	B3-198-3
	5	330	15.2	198	165	280.5	B1-198-5	215	305.25	B2-198-5	264	330	B3-198-5
	10	330	30.3	198	165	280.5	B1-198-10	215	305.25	B2-198-10	264	330	B3-198-10
	15	330	45.5	198	165	280.5	B1-198-15	215	305.25	B2-198-15	264	330	B3-198-15
	3	330	9.1	330	165	412.5	B1-330-3	215	437.25	B2-330-3	264	462	B3-330-3
	5	330	15.2	330	165	412.5	B1-330-5	215	437.25	B2-330-5	264	462	B3-330-5
	10	330	30.3	330	165	412.5	B1-330-10	215	437.25	B2-330-10	264	462	B3-330-10
	15	330	45.5	330	165	412.5	B1-330-15	215	437.25	B2-330-15	264	462	B3-330-15
	3	330	9.1	462	165	544.5	B1-462-3	215	569.25	B2-462-3	264	594	B3-462-3
	5	330	15.2	462	165	544.5	B1-462-5	215	569.25	B2-462-5	264	594	B3-462-5
	10	330	30.3	462	165	544.5	B1-462-10	215	569.25	B2-462-10	264	594	B3-462-10
	15	330	45.5	462	165	544.5	B1-462-15	215	569.25	B2-462-15	264	594	B3-462-15
C	3	450	6.7	270	225	382.5	C1-270-3	293	416.25	C2-270-3	360	450	C3-270-3
	5	450	11.1	270	225	382.5	C1-270-5	293	416.25	C2-270-5	360	450	C3-270-5
	10	450	22.2	270	225	382.5	C1-270-10	293	416.25	C2-270-10	360	450	C3-270-10
	15	450	33.3	270	225	382.5	C1-270-15	293	416.25	C2-270-15	360	450	C3-270-15
	3	450	6.7	450	225	562.5	C1-450-3	293	596.25	C2-450-3	360	630	C3-450-3
	5	450	11.1	450	225	562.5	C1-450-5	293	596.25	C2-450-5	360	630	C3-450-5
	10	450	22.2	450	225	562.5	C1-450-10	293	596.25	C2-450-10	360	630	C3-450-10
	15	450	33.3	450	225	562.5	C1-450-15	293	596.25	C2-450-15	360	630	C3-450-15
	3	450	6.7	630	225	742.5	C1-630-3	293	776.25	C2-630-3	360	810	C3-630-3
	5	450	11.1	630	225	742.5	C1-630-5	293	776.25	C2-630-5	360	810	C3-630-5
	10	450	22.2	630	225	742.5	C1-630-10	293	776.25	C2-630-10	360	810	C3-630-10
	15	450	33.3	630	225	742.5	C1-630-15	293	776.25	C2-630-15	360	810	C3-630-15
D	5	500	10	300	250	425	D1-300-5	325	462.5	D2-300-5	400	500	D3-300-5
	10	500	20	300	250	425	D1-300-10	325	462.5	D2-300-10	400	500	D3-300-10
	15	500	30	300	250	425	D1-300-15	325	462.5	D2-300-15	400	500	D3-300-15
	20	500	40	300	250	425	D1-300-20	325	462.5	D2-300-20	400	500	D3-300-20
	5	500	10	500	250	625	D1-500-5	325	662.5	D2-500-5	400	700	D3-500-5
	10	500	20	500	250	625	D1-500-10	325	662.5	D2-500-10	400	700	D3-500-10
	15	500	30	500	250	625	D1-500-15	325	662.5	D2-500-15	400	700	D3-500-15
	20	500	40	500	250	625	D1-500-20	325	662.5	D2-500-20	400	700	D3-500-20
	5	500	10	700	250	825	D1-700-5	325	862.5	D2-700-5	400	900	D3-700-5
	10	500	20	700	250	825	D1-700-10	325	862.5	D2-700-10	400	900	D3-700-10
	15	500	30	700	250	825	D1-700-15	325	862.5	D2-700-15	400	900	D3-700-15

	20	500	40	700	250	825	D1-700-20	325	862.5	D2-700-20	400	900	D3-700-20
E	5	600	8.3	360	300	510	E1-360-5	390	555	E2-360-5	480	600	E3-360-5
	10	600	16.7	360	300	510	E1-360-10	390	555	E2-360-10	480	600	E3-360-10
	15	600	25	360	300	510	E1-360-15	390	555	E2-360-15	480	600	E3-360-15
	20	600	33.3	360	300	510	E1-360-20	390	555	E2-360-20	480	600	E3-360-20
	5	600	8.3	600	300	750	E1-600-5	390	795	E2-600-5	480	840	E3-600-5
	10	600	16.7	600	300	750	E1-600-10	390	795	E2-600-10	480	840	E3-600-10
	15	600	25	600	300	750	E1-600-15	390	795	E2-600-15	480	840	E3-600-15
	20	600	33.3	600	300	750	E1-600-20	390	795	E2-600-20	480	840	E3-600-20
	5	600	8.3	840	300	990	E1-840-5	390	1035	E2-840-5	480	1080	E3-840-5
	10	600	16.7	840	300	990	E1-840-10	390	1035	E2-840-10	480	1080	E3-840-10
	15	600	25	840	300	990	E1-840-15	390	1035	E2-840-15	480	1080	E3-840-15
	20	600	33.3	840	300	990	E1-840-20	390	1035	E2-840-20	480	1080	E3-840-20

4.3. Mesh convergence study

The RBS1 model was used to conduct a mesh convergence study. Four different mesh sizes: coarse, medium, fine and very fine (**Figure 7**) were used for the evaluation. The results showed that the simulations using a fine and a very fine mesh presented yield similar results **(Figure 8)** in terms of the maximum moment, thus fine mesh size was chosen to model the plastic zone region of the beams where stresses are high for all FE models. As it was described before, the four-node doubly curved shell element (S4R) with reduced integration was employed.

4.4. Loading sequence

The SAC loading protocol (FEMA 350, 2000) previously shown in **Figure 4** and the corresponding displacements based on the test setup, load step, and beam span are summarised in **Table 7**.

4.5. Analysis

A nonlinear (geometric and material) static analysis with the full Newton-Raphson approach and direct method for the equation solver was employed by ABAQUS 6.14 (2014). The increment size of the sub-steps was automatically controlled by the program to help prevent convergence issues. To prevent premature Lateral Torsional Buckling (LTB) of the long beams, a lateral restraint has been provided at 1.5 m to 2.5 m intervals; alike with concrete slab presence which would prevent the beams from failing in the out-of-plane.

The moment-rotation hysteretic curves produced are referring to the total rotation of the beam at beam end after the full 32 cycles. The rotations were calculated by dividing the vertical displacements by the distance to column face.

Table 7. Load step and the results of end displacement of the beams.

Load Step				1	2	3	4	5	6	7	8	9
Cycle Number				1-6	6-12	12-18	18-22	22-24	24-26	26-28	28-30	30-32
Number of Cycles				6	6	6	4	2	2	2	2	2
Peak Rotation φ				0.00375	0.005	0.0075	0.01	0.015	0.02	0.03	0.04	0.05
Setup	Span m	hc m	L_{CL} m	**Beam end displacements (**mm) $\Delta L_{CL}=\varphi*L_{CL}$								
A	2	0.30	1.15	4.31	5.75	8.63	11.50	17.25	23.00	34.50	46.00	57.50
B HE300 B	3	0.30	1.65	6.19	8.25	12.38	16.50	24.75	33.00	49.50	66.00	82.50
	5	0.30	2.65	9.94	13.25	19.88	26.50	39.75	53.00	79.50	106.00	132.50
	10	0.30	5.15	19.31	25.75	38.63	51.50	77.25	103.00	154.50	206.00	257.50
	15	0.30	7.65	28.69	38.25	57.38	76.50	114.75	153.00	229.50	306.00	382.50
C HE450 B	3	0.45	1.73	6.47	8.63	12.94	17.25	25.88	34.50	51.75	69.00	86.25
	5	0.45	2.73	10.22	13.63	20.44	27.25	40.88	54.50	81.75	109.00	136.25
	10	0.45	5.23	19.59	26.13	39.19	52.25	78.38	104.50	156.75	209.00	261.25
	15	0.45	7.73	28.97	38.63	57.94	77.25	115.88	154.50	231.75	309.00	386.25
D HE500 B	3	0.50	1.75	6.56	8.75	13.13	17.50	26.25	35.00	52.50	70.00	87.50
	5	0.50	2.75	10.31	13.75	20.63	27.50	41.25	55.00	82.50	110.00	137.50
	10	0.50	5.25	19.69	26.25	39.38	52.50	78.75	105.00	157.50	210.00	262.50
	15	0.50	7.75	29.06	38.75	58.13	77.50	116.25	155.00	232.50	310.00	387.50
E HE650 B	3	0.65	1.83	6.84	9.13	13.69	18.25	27.38	36.50	54.75	73.00	91.25
	5	0.65	2.83	10.59	14.13	21.19	28.25	42.38	56.50	84.75	113.00	141.25
	10	0.65	5.33	19.97	26.63	39.94	53.25	79.88	106.50	159.75	213.00	266.25
	15	0.65	7.83	29.34	39.13	58.69	78.25	117.38	156.50	234.75	313.00	391.25

Setup A is the one used for the RBS1 (verification) model.
L_{CL} = Span/2+h_c/2 (see **Figure 4**)

5. Results and discussions

5.1. Results

The results from the quasi-static hysteretic graphs of the studied specimens are summarised in this section. For every connection under investigation, another extra connection using solid-webbed beams is introduced to form a fair comparison and draw better conclusions with regards to the performance of the RWS connections.

M_y is the yield moment and M_u is the ultimate moment in kNm obtained from the hysteresis curve and calculated as $M=P*L$, where L is the distance between load axis and the column face axis and P is the reaction force. θ_y is the yielding rotation and θ_u is the ultimate rotation in rads (displacement over distance). Rotational ductility D_θ, is calculated by dividing the ultimate rotation by the yielding rotation ($D_\theta=\theta_u/\theta_y$). High rotational ductility under cyclic loading refers to the post-peak deformability of members under seismic load, which usually supports the members to dissipate more seismic energy by the connection through forming a plastic hinge. Initial rotational stiffness (K_i) is calculated by dividing the first cycle's moment over its rotation ($K_i=M/\theta$). WOA is the total web opening area of the beam in mm^2. Estimated energy dissipation capacity ($E_{i,max}$), is the area inside the ultimate moment-rotation hysteresis curve (M_u and θ_u) in kNm.rad. d_0 is the opening diameter in mm. Yield moment ratio (M_{yR}), is the ratio of the yield moment (M_y) to the yield moment of the corresponding solid beam.

The span over depth ratio (S/h), is the ratio of the beam span over its total depth (section height), which has a significant influence on the behaviour of the connection and the type of plastic hinge (see section 5.1.1). M_{yEC} is the yield moment as calculated according to Eurocode 3 for the connection with the solid-webbed beam. The ratio of the moment estimated from the FE analysis yield and the moment calculated from Eurocode 3 is also computed to find the estimated yielding moment of the RWS connections as follows: $M_{yFE(Solid)}/M_{yEC3(Solid)}$ = a, thus $M_{yEC3}=M_{yFE}/a$. The results of the verification specimen RBS1 are summarised in **Table 8**.

Table 8. Verification model results.

Specimen	Span /h	d_0 (mm)	M_y (kNm)	M_u (kNm)	θ_y (rad)	θ_u (rad)	D_θ	K_i (kNm/rad)	WOA (cm^2)	$E_{i,max}$ (kNm.rad)	M_{yEC} (kNm)	M_{yR}	CFS	PHS
Solid-webbed	8.7	0	228.4	285.6	0.0131	0.0531	4.05	21685	-	60.6	227.2	1.00	VH	CF
RBS1	8.7	0	173.7	263.6	0.0098	0.0547	5.58	19338	-	57.6	172.8	0.76	M	F

5.1.1. *Plastic Hinge Formation (PHF)*

The Plastic Hinge Formation (PHF) was observed through the FE analyses. For the ease of understanding the PHF is divided into four categories that represent the extent of the plastic hinge formation in the beam as follows: O for minor hinge in the vicinity of the web opening, P for partial plastic hinge formation, F for full plastic hinge formation (flanges are fully yielded too), and CF for plastic hinge formation at column face, as denoted in **Figure 9**.

5.1.2. *Column Face Stress (CFS)*

Column Face Stress (CFS) was observed through the FE analyses, which is divided into four categories that represent the stress level at the column face as follows: L for low stress, M for moderate stress, H for high stress, and VH for very high stress. An example of each CFS tabulated in Table 20 is shown in **Figure 10** to visualise the stress levels at the point where the beam flange meets the column flange (welding zone) in order to understand the inelastic behaviour of the connection and the perforated beam in comparison with the inelastic capacity of the welding zone. When high or very high stresses are concentrated in the welding zone, the structural integrity of the connection is under threat as the inelastic capacity of welds is low and a sudden welding fracture may occur. In that scenario, the effect of the RWS connection was minimal to negligible and an unreliable design for seismic resistance.

The main results of all test setup specimens are summarised in Table 20 in the Appendix.

5.2. Discussion

As it was aforementioned, a linear interpolation method was employed to draw the results for the connections which were not modelled. There is no extrapolation of the results since it is not recommended based on FEMA 350 (2000) and AISC 358 (2010).

5.2.1. *Ultimate moment capacity*

As expected, the connections with solid-webbed beams achieved higher moment capacities. In RWS connections, the decrease of the moment capacity was observed which was directly related to the opening size and its position as well as the beam span. By increasing the web opening depth, d_0,

the moment capacity decreases – not as much as the shear capacity decreases, and by increasing the web opening end distance, *S*, the moment capacity increases since a (shear) plastic hinge is less likely to be formed (**Figure 11)**. However, it is worth to note that in such circumstances, the "strong" connections may fail suddenly by the low inelasticity of the welding, therefore the RBS and RWS design concept which reduces the capacity of the beam by increasing its inelasticity and thus the connection's ductility. The lowest moment capacity was observed for opening type 3 which has a d_0 of 0.80h with only 45% of the moment capacity of the reference connection with the solid-webbed beam.

It is observed that for specific opening size when increasing the end distance from the column face of the column the beam capacity increases for all specimens (**Figure 11)**. Also, when the web opening size increases, the moment capacity of larger spans is higher compared with shorter spans because of the shear capacity reduction which is more apparent in short span beams. For examples, for test setup B and for opening category 1, the moment capacity ratio of 15 m to 3 m span was 0.89, while for opening category 3 the same ratio was 1.21. Almost for all connections, increasing the end distance of the opening from column face, *S*, results in increased moment capacity of the connection; about 7% of an increase could be realised in all models. The effect of the parameters on the moment capacity, starting with the most significant, are d_0 with 30%, *S* with 7%, and beam's span with 3% of moment capacity reduction. Moreover, larger web openings have a lower effect on strength degradation. All ultimate moments have been summarised in Table 9.

Table 9. Ultimate moments values.

Opening Category	Opening Distance	Setup B		Setup C		Setup D		Setup E	
		Specimen	M_u	Specimen	M_u	Specimen	M_u	Specimen	M_u
Solid-webbed		B-Solid-3	330.8	C-Solid-3	856.0	D-Solid-5	1098.9	E-Solid-5	1561.3
Opening 1 d_0=0.50h	S_h=0.87h	B1-287-3	293.7	C1-392-3	655.3	D1-435-5	847.9	E1-522-5	1367.4
		B1-287-15	273.4	C1-392-15	635.4	D1-435-20	785.9	E1-522-20	1097.9
	S_h=1.74h	B1-574-3	315.8	C1-783-3	737.1	D1-870-5	1030.7	E1-1044-5	1538.3
		B1-574-15	269.9	C1-783-15	636.1	D1-870-20	790.6	E1-1044-20	1151.0
Opening 2 d_0=0.65h	S_h=0.87h	B2-287-3	251.2	C2-392-3	519.0	D2-435-5	730.6	E2-522-5	1171.8
		B2-287-15	270.7	C2-392-15	627.4	D2-435-20	745.8	E2-522-20	1206.5
	S_h=1.74h	B2-574-3	292.2	C2-783-3	603.8	D2-870-5	835.5	E2-1044-5	1290.3
		B2-574-15	271.8	C2-783-15	630.6	D2-870-20	779.7	E2-1044-20	1179.9
Opening 3 d_0=0.80h	S_h=0.87h	B3-287-3	175.5	C3-392-3	330.3	D3-435-5	526.6	E3-522-5	797.0
		B3-287-15	219.2	C3-392-15	460.5	D3-435-20	602.3	E3-522-20	906.2
	S_h=1.74h	B3-574-3	192.2	C3-783-3	362.3	D3-870-5	578.6	E3-1044-5	882.9
		B3-574-15	227.4	C3-783-15	483.8	D3-870-20	629.9	E3-1044-20	941.8

5.2.2. *Yielding moment capacity*

The effect of parameters on the yielding moment capacity, starting with the most significant, are d_0, beam span, and *S* with about 16%, 10%, and 5%, respectively. Overall, as shown in Table 10 is different from that of it is noted that in the specimens with short spans (i.e., 3 m and 5 m) the yielding happens around cycle 18 while in the one with longer spans yielding happens around cycle 26 due to the lower significance of the reduced shear capacity resulted from the web opening presence. It is worth to clarify that RWS connections fail with a shear plastic hinge formation as opposed to the moment plastic hinge formation observed in RBS connections.

Table 10. Yielding moment values.

Opening Category	Opening Distance	Setup B		Setup C		Setup D		Setup E	
		Specimen	M_y	Specimen	M_y	Specimen	M_y	Specimen	M_y
Solid-webbed		B-Solid-3	245.3	C-Solid-3	580.1	D-Solid-5	698.3	E-Solid-5	1181.1
Opening 1 d_0=0.50h	S_h=0.87h	B1-287-3	238.8	C1-392-3	535.1	D1-435-5	668.6	E1-522-5	1111.5
		B1-287-15	230.3	C1-392-15	497.3	D1-435-20	642.7	E1-522-20	974.8
	S_h=1.74h	B1-574-3	247.8	C1-783-3	562.4	D1-870-5	695.8	E1-1044-5	1164.3
		B1-574-15	242.4	C1-783-15	507.9	D1-870-20	667.6	E1-1044-20	1002.9
Opening 2 d_0=0.65h	S_h=0.87h	B2-287-3	215.3	C2-392-3	462.9	D2-435-5	600.4	E2-522-5	1009.0
		B2-287-15	220.8	C2-392-15	466.4	D2-435-20	600.7	E2-522-20	920.0
	S_h=1.74h	B2-574-3	235.3	C2-783-3	511.7	D2-870-5	683.4	E2-1044-5	1124.8
		B2-574-15	228.2	C2-783-15	497.8	D2-870-20	634.5	E2-1044-20	959.1
Opening 3 d_0=0.80h	S_h=0.87h	B3-287-3	163.4	C3-392-3	309.4	D3-435-5	496.6	E3-522-5	759.3
		B3-287-15	204.9	C3-392-15	423.0	D3-435-20	555.1	E3-522-20	828.4
	S_h=1.74h	B3-574-3	173.8	C3-783-3	327.0	D3-870-5	535.7	E3-1044-5	822.0
		B3-574-15	212.5	C3-783-15	447.5	D3-870-20	577.4	E3-1044-20	883.3

5.2.3. *Dissipated energy*

The dissipated energy of the connections is the sum of the area under M-θ curve for all loading steps which takes into account the exact shape of the hysteresis curve and is dependent on both the moment capacity and ultimate rotational capacity of the connections. Since the test is 'displacement control', all the specimens presented a similar ultimate rotation which will make the dissipated energy dependent on the ultimate moment; the higher the ultimate moment the more energy dissipated. What is important in energy dissipation is, how well the connections can absorb the energy without stressing the column face area and without excessive degradation. For the purpose of proposedly shifting the plastic hinge to the desired location (here web opening) the beam must lose a considerate portion of its moment resistance at this section (30-40%). It is observed that as the web opening size increases the dissipated energy increases. As the web opening end distance increases the dissipated energy decreases, despite the ultimate moment increase. Increasing beam span reduces dissipated energy as the RWS effect becomes less significant. In contrast, RWS connections with large web openings yield higher energy dissipation over the ultimate moment (Table 11).

Table 11. Dissipated energy values.

Setup F				
Specimen	Mu	E	M/M_{solid}	E/M_u
F-solid-1.6	110.36	59.2	1.00	0.54
F2-185-1.6	72.59	47.7	0.66	0.66
F2-185-6	83.96	34.4	0.76	0.41
F2-345-1.6	83.03	47.8	0.75	0.58
F2-345-6	84.91	34.1	0.77	0.40
F3-200-1.6	48.90	32.7	0.44	0.67
F3-200-6	61.98	26.9	0.56	0.43
F3-360-1.6	53.79	36.2	0.49	0.67
F3-360-6	65.17	27.5	0.59	0.42

5.2.4. *Column face stress level*

The efficient design of RWS connections manages to mobilise stresses away from the column shear panel zone and the (moment) weld between the beam and column to the vicinity of the web openings where usually four local plastic hinges are formed. Connections with solid-webbed beams fully-welded to deep-column flange demonstrate an undesirable behaviour due to the inelasticity demand during an earthquake which cannot be provided by the weld. Examining the effect of the web opening size, larger web openings result in the reduction of the yielding load, although higher stresses appear in the vicinity of the web opening and a lower stress level at column face (**Figure 12**).

With regards to the effect of the end distance of the web opening from the column face, different results are concluded (Table 12) looking at different opening sizes (i.e., different end distances). While increasing the opening size it mobilises the stress away from column face; the presence of an opening in specimen B1-574-3 resulted in stress distribution in the vicinity of the opening, as well as stress concentration around the welding region due to the narrow end distance. It results that the most critical factor is the opening height.

Table 12. Column face stress level.

Opening Category	Opening Distance	Setup B		Setup C		Setup D		Setup E	
		Specimen	CFS	Specimen	CFS	Specimen	CFS	Specimen	CFS
Solid-webbed		B-Solid-3	VH	C-Solid-3	VH	D-Solid-5	VH	E-Solid-5	VH
Opening 1 d_0=0.50h	S_h=0.87h	B1-287-3	M	C1-392-3	M	D1-435-5	M	E1-522-5	M
		B1-287-15	M	C1-392-15	M	D1-435-20	M	E1-522-20	M
	S_h=1.74h	B1-574-3	VH	C1-783-3	VH	D1-870-5	VH	E1-1044-5	VH
		B1-574-15	H	C1-783-15	H	D1-870-20	H	E1-1044-20	H
Opening 2 d_0=0.65h	S_h=0.87h	B2-287-3	M	C2-392-3	M	D2-435-5	M	E2-522-5	M
		B2-287-15	M	C2-392-15	M	D2-435-20	M	E2-522-20	M
	S_h=1.74h	B2-574-3	L	C2-783-3	L	D2-870-5	L	E2-1044-5	L
		B2-574-15	M	C2-783-15	M	D2-870-20	M	E2-1044-20	M
Opening 3 d_0=0.80h	S_h=0.87h	B3-287-3	L	C3-392-3	L	D3-435-5	L	E3-522-5	L
		B3-287-15	L	C3-392-15	L	D3-435-20	L	E3-522-20	L
	S_h=1.74h	B3-574-3	L	C3-783-3	L	D3-870-5	L	E3-1044-5	L
		B3-574-15	L	C3-783-15	L	D3-870-20	L	E3-1044-20	L

5.2.5. *Analysis of PHF*

Connections using solid-webbed beams show a significant stress concentration near the welding zone and the beam flanges. As presented in section 5.1.1, PHF is divided into four categories such as yielding at column face (CF), full plastic hinge (F), a small area around the opening (O) and partially (P). RWS connections with small web openings do not manage to efficiently mobilise the stresses away from the welding area. Especially when the beam has a large span, the shear reduction due to the small web openings is significantly lower and the plastic hinge of the beam is formed near the face of the column as shown in **Figure 13**. Specimens with O and P type of plastic hinges always have longer spans, while the specimens were not fully yielded at the end of the SAC protocol, i.e., 32-cycle peak deformation. Table 13 summarises the PHF types observed during the analytical studies.

Table 13. Plastic hinge formation types.

Opening Category	Opening Distance	Setup B		Setup C		Setup D		Setup E	
		Specimen	PHS	Specimen	PHS	Specimen	PHS	Specimen	PHS
Solid-webbed		B-Solid-3	CF	C-Solid-3	CF	D-Solid-5	CF	E-Solid-5	CF
Opening 1 0.50h	Sh=0.87h	B1-287-3	F	C1-392-3	F	D1-435-5	F	E1-522-5	F
		B1-287-15	O	C1-392-15	O	D1-435-20	O	E1-522-20	F
	Sh=1.74h	B1-574-3	CF	C1-783-3	F	D1-870-5	F	E1-1044-5	F
		B1-574-15	CF	C1-783-15	O	D1-870-20	O	E1-1044-20	P
Opening 2 0.65h	Sh=0.87h	B2-287-3	F	C2-392-3	F	D2-435-5	F	E2-522-5	F
		B2-287-15	O	C2-392-15	P	D2-435-20	P	E2-522-20	P
	Sh=1.74h	B2-574-3	F	C2-783-3	F	D2-870-5	F	E2-1044-5	F
		B2-574-15	O	C2-783-15	P	D2-870-20	P	E2-1044-20	P
Opening 3 0.80h	Sh=0.87h	B3-287-3	F	C3-392-3	F	D3-435-5	F	E3-522-5	F
		B3-287-15	F	C3-392-15	F	D3-435-20	F	E3-522-20	F
	Sh=1.74h	B3-574-3	F	C3-783-3	F	D3-870-5	F	E3-1044-5	F
		B3-574-15	F	C3-783-15	F	D3-870-20	F	E3-1044-20	F

5.2.6. *Local web buckling*

Local beam web buckling is observed approximately after cycle 26 in opening category 1 and strength degradation follows – usually around cycle 26 which has a peak deformation of 0.03rad (**Figure 14**). Web local buckling was mainly observed in the vicinity of small openings (d_0=0.50h) due to high shear strength found, thus higher forces. Connections with medium size web openings (d_0=0.65h) failed by a combination of the Vierendeel mechanism (Tsavdaridis and D'Mello, 2012) which happens first and then some local web buckling takes place. Connections with large web openings (d_0=0.80h) fail predominately by the Vierendeel mechanism, and minor web buckling is then observed (**Figure 12**). It is worth to note that the clear development of the Vierendeel mechanism is demonstrated by the formation of the four plastic hinges at the edge of the opening.

However, cases where high-stress concentration is found in such plastic hinges at the edge of the web opening which can lead to steel fracture when large displacements are applied. Such failure behaviour was also observed in the experimental study of Yang et al (2009) (**Figure 15**).

5.2.7. *Vierendeel mechanism*

Formation of Vierendeel moment (i.e., four plastic hinges in the vicinity of the web opening) results from the action of shear force in the tee-sections over the horizontal length of the web opening (which defines the critical opening length), therefore, the width of the web opening directly influences the Vierendeel mechanism failure. Vierendeel mechanism mostly happens when large web openings while in small openings the dominant failure type is local web buckling. Vierendeel mechanism has the capacity to mobilises the stress away from the critical connection zone (shear panel and welding area) while it provides ductility to the connection, thus seismic energy is dissipated and the welds are not prone to fail inelastically. Along with the Vierendeel mechanism formation, the onset of strength degradation of the connection may take place as shown in **Figure 16**.

6. RWS connection design procedure

6.1. Introduction

AISC 358 (2010) includes one chapter for every pre-qualified connection. Due to many similarities between RBS connections and RWS connections, chapter 5 of AISC 358-10 is used to propose a design procedure for RWS connections in the current study. Due to some uncertainty in the performance of RWS connections with opening category 1 (d_0=0.5h) as observed by Table 12 and Table 13, this particular category was not taken into consideration when developing the design procedure. In general, RWS connections with small web openings are inefficient and often impractical, thus no more reference for them will be made.

6.2. Design procedure

6.2.1. **Step 1.** Choose trial values for the column and beam sections, d_0 and S of the web opening (***Figure 6***) subject to the limits:

$$0.65h \leq d_0 \leq 0.8h$$

$$0.60h \leq S \leq 1.40h$$

Where:
h = overall height of the beam, mm.
d_0 = opening height of the RWS cut, mm.
S = horizontal distance from the face of column flange to the start of the RWS cut, mm.

Confirm that the beams and columns are adequate for all load combinations specified by the applicable building code, including the reduced section of the beam (recommended by SCI P355, 2011), and that the design story drift for the frame complies with applicable limits specified by the corresponding building code. The calculation of elastic drift shall consider the effect of the reduced web section.

6.2.2. **Step 2.** Compute the plastic section modulus at the centre of the reduced web section:

AISC 358-10 suggests the calculation of plastic section modulus at the centre of the reduced beam section by deducting the cut section from the full beam cross-section. It proposes this method to calculate the plastic section modulus and plastic moment. Using this method, the plastic moment was calculated for E-Solid-5, E1-522-5, E2-522-5, E3-522-5 and the results were compared against finite element moments to validate this method.

Table 14. AISC and FE moment comparison.

Specimen	r (mm)	Z_{RWS} (cm^3)	AISC M_{pl} (kN.m)	FE M_{pl} (kN.m)	Error
E-Solid-5	-	3512	1071	1181	10.3%
E1-522-5	150	3342	989	1111	12.3%
E2-522-5	195	3056	932	1009	8.3%
E3-522-5	240	2821	860	759	-11.7%

Observing the results in Table 14, it is concluded that the plastic moment cannot be calculated by simply calculating the plastic modulus of the reduced section. For example, in connections with

opening category 1, the calculated moment is 12.3% lower than the one computed from the FE model, while in opening category 3 it is 11.7% higher. Since RBS connections fail by one failure mode, this method could be practical and accurate. However, RWS connections fail differently, for example increasing the opening height will change the failure mechanism from local web buckling to Vierendeel mechanism, which eventually results in a different moment capacity of the connection. Hence, a factor based method is proposed for calculating the plastic moment. Table 20 figures were refined and interpolated to get the moment ratio to the plastic moment of the solid beam. At this stage, more test setups (data points) were needed to achieve more accurate moment ratios, consequently, four extra beam sizes were modelled and analysed to strengthen the reliability of the moment ratios. Again, RWS connections with a small web opening (d_0=0.5h) were ignored due to poor behaviour while high stresses were found at column face. Information on the new test specimens is tabulated in Table 15.

Table 15. New test specimens.

Test Setup	Span (m)	h (mm)	Span /h	S (mm)	Opening **2**, d_0=0.65h			Opening **3**, d_0=0.80h		
					d_0	S_h	Setup	d_0	S_h	Setup
F	1.6	200	8	120	130	185	F2-185-1.6	160	200	F3-200-1.6
	6	200	30	120	130	185	F2-185-6	160	200	F3-200-6
	1.6	200	8	200	130	265	F2-265-1.6	160	280	F3-280-1.6
	6	200	30	200	130	265	F2-265-6	160	280	F3-280-6
	1.6	200	8	280	130	345	F2-345-1.6	160	360	F3-360-1.6
	6	200	30	280	130	345	F2-345-6	160	360	F3-360-6
G	1.92	240	8	144	156	222	G2-222-1.92	192	240	G3-240-1.92
	7.2	240	30	144	156	222	G2-222-7.2	192	240	G3-240-7.2
	1.92	240	8	240	156	318	G2-318-1.92	192	336	G3-336-1.92
	7.2	240	30	240	156	318	G2-318-7.2	192	336	G3-336-7.2
	1.92	240	8	336	156	414	G2-414-1.92	192	432	G3-432-1.92
	7.2	240	30	336	156	414	G2-414-7.2	192	432	G3-432-7.2
H	2.16	270	8	162	176	250	H2-250-2.16	216	270	H3-270-2.16
	8.1	270	30	162	176	250	H2-250-8.1	216	270	H3-270-8.1
	2.16	270	8	270	176	358	H2-358-2.16	216	378	H3-378-2.16
	8.1	270	30	270	176	358	H2-358-8.1	216	378	H3-378-8.1
	2.16	270	8	378	176	466	H2-466-2.16	216	486	H3-486-2.16
	8.1	270	30	378	176	466	H2-466-8.1	216	486	H3-486-8.1
I	6	750	8	450	488	694	I2-694-6	600	750	I3-750-6
	22.5	750	30	450	488	694	I2-694-22.5	600	750	I3-750-22.5
	6	750	8	750	488	994	I2-994-6	600	1050	I3-1050-6
	22.5	750	30	750	488	994	I2-994-22.5	600	1050	I3-1050-22.5
	6	750	8	1050	488	1294	I2-1294-6	600	1350	I3-1350-6
	22.5	750	30	1050	488	1294	I2-1294-22.5	600	1350	I3-1350-22.5

Combining the results from the new test specimens and the ones presented earlier in this paper, the moment ratios are calculated and summarised in Table 16. Linear interpolation between specimens with different opening sizes is not recommended due to its nonlinear behaviour (**Figure 11b**), but it is acceptable within specimens with different opening end distance due to its linear trend (**Figure 11a**) Thus, linear interpolation was employed to increase the range of span sizes and opening distances included in this study and be available to be used by practicing engineers.

Step 2.1 Compute the plastic moment of the full beam cross section (Solid).

$$M_{pl,\,Solid} = Z_x * f_y$$

Where:

Z_x = plastic section modulus about the x-axis, for full beam cross-section, mm^3.

f_y = specified minimum yield stress of the yielding element, MPa (N/mm^2)

Step 2.2 Compute the plastic moment of the reduced web section.

$$M_{pl} = M_{pl,\,Solid} * C$$

Where:

$M_{pl,\,Solid}$ = Plastic moment of the solid beam, MPa (N/mm^2)

C = Plastic moment factor, tabulated in Table 16

For the web opening end distance (S), span and beam heights are not presented in the table; linear interpolation may be used to get the moment factor.

Table 16. Plastic moment factor (C).

Span/ depth	**$My/M_{pl,Solid}$**					
	d_0 = 0.65h			**d_0 = 0.80h**		
	S			**S**		
	0.4h	**1.0h**	**1.4h**	**0.4h**	**1.0h**	**1.4h**
8	0.84	0.87	0.89	0.59	0.62	0.64
12	0.85	0.88	0.90	0.63	0.66	0.68
16	0.86	0.88	0.91	0.67	0.69	0.72
20	0.87	0.89	0.92	0.70	0.73	0.75
24	0.88	0.90	0.92	0.74	0.76	0.79
30	0.89	0.91	0.94	0.79	0.81	0.84

6.2.3. **Step 3.** Compute the probable maximum moment, M_{pr}, at the centre of the reduced section:

$$M_{pr} = C_{pr} * R_y * M_{pl}$$

Where:

R_y = ratio of the expected yield stress to the specified minimum yield stress f_y as specified in the AISC Seismic Provisions (Table 5-14) here Table 17

C_{pr} = factor to account for the peak connection strength, including strain hardening, local restraint, additional reinforcement, and other connection conditions. The value of C_{pr} shall be:

$$C_{pr} = \frac{f_u + f_y}{2f_y} \leq 1.2$$

C_{pr} = factor to account for the peak connection strength, including strain hardening, local restraint, additional

f_y = specified minimum yield stress of the yielding element, MPa (N/mm^2)

f_u = specified minimum tensile strength of the yielding element, MPa (N/mm^2)

*Table 17. R_y values **(AISC 341, 2010)**.*

Application	R_y
Hot-rolled structural shapes and bars:	
• ASTM A36/A36M	1.5
• ASTM A1043/1043M Gr. 36 (250)	1.3
• ASTM A572/572M Gr. 50 (345) or 55 (380), ASTM A913/913M Gr. 50 (345), 60 (415), or 60 (450), ASTM A588/588M, ASTM A992/992M	1.1
• ASTM A1043/1043M Gr. 50 (345)	1.2
• ASTM A529 Gr. 50 (345)	1.2
• ASTM A529 Gr. 55 (380)	1.1
Hollow structural sections (HSS):	
• ASTM A500/A500M (Gr. B or C), ASTM A501	1.4
Pipe:	
• ASTM A53/A53M	1.6
Plates, Strips and Sheets:	
• ASTM A36/A36M	1.3
• ASTM A1043/1043M Gr. 36 (250)	1.3
• A1011/A1011M HSLAS Gr. 55 (380)	1.1
• ASTM A572/572M Gr. 42 (290)	1.3
• ASTM A572/572M Gr. 50 (345), Gr. 55 (380), ASTM A588/588M	1.1
• ASTM A1043/1043M Gr. 50 (345)	1.2
Steel Reinforcement:	
• ASTM A615, ASTM A706	1.25

6.2.4. **Step 4.** Compute the shear force at the centre of the reduced web sections at each end of the beam:

The shear force at the centre of the reduced web sections shall be determined from a free body diagram of the portion of the beam between the centres of the reduced web sections (AISC 358, 2010). This calculation shall assume the moment at the centre of each reduced web section is M_{pr} and shall include gravity loads acting on the beam based on the load combination $1.2D + f_1L + 0.2S$, where f_1 is the load factor determined by the applicable building code for live loads, but not less than 0.5.

6.2.5. ***Step 5.*** *Compute the probable maximum moment at the face of the column.*

The moment at the face of the column shall be computed from a free-body diagram of the segment of the beam between the centre of the reduced section and the face of the column, as illustrated in **Figure 17**.

Based on this free-body diagram, the moment at the face of the column is computed as follows:

$$M_f = M_{pr} + V_{RWS} * S_h$$

Where:

M_f = probable maximum moment at the face of column, kip-in. (N-mm)

S_h = distance from face of the column to the plastic hinge, in. (mm)

= S+r, in. (mm)

V_{RWS} = larger of the two values of shear force at the centre of the reduced section at each end of the beam, kips (N).

This equation ignores the gravity load on the portion of the beam between the centre of the reduced web section and the face of the column. If desired, the gravity load on this small portion of the beam is permitted to be included in the free-body diagram shown in **Figure 17**.

6.2.6. **Step6.** Compute M_{pe}, the plastic moment of the beam based on the expected yield stress:

$$M_{pe} = M_{pl,\,Solid} * R_y$$

6.2.7. **Step7.** Check the flexural strength of the beam at the face of the column:

$$Mf \leq \varphi_d * M_{pe}$$

Where:

φ_d = resistance factor for ductile limit states

= 1.00

If this equation is not satisfied, adjust the values of d_0 and S, or adjust the section size, and repeat Steps 2 through 7.

6.2.8. **Step 8.** Determine the required shear strength, V_u, of a beam and beam web-to-column connection from:

$$V_u = \frac{2M_{pr}}{L_h} + V_{gravity}$$

Where:

V_u = required shear strength of beam and beam web-to-column connection, N

L_h = distance between plastic hinge locations, mm

$V_{gravity}$ = beam shear force resulting from $1.2D + f_1L + 0.2S$ (where: f_1 is the load factor determined by the applicable building code for live loads, but not less than 0.5), N

Check design shear strength of beam according to Chapter G of the AISC Specification. (AISC 360, 2010)

Reduced shear strength of the beam at the centreline of the opening is adequate to withstand the gravity loads but higher shear forces are accounted as a result of the seismic action. When the reduced section is subjected to a seismic action or cyclic loading, this inherent low shear strength may result in fracture of the beam web in the vicinity of the web opening due to high concentration of stresses; buckled edge was also observed in the experimental study of Yang et al. (2009) which is shown in **Figure 14**.

6.2.9. **Step 9.** Design the beam web-to-column connection according to Section 5.6. *(AISC 358, 2010)*

6.2.10. **Step 10.** Check continuity plate requirements according to Chapter 2. *(AISC 358, 2010)*

6.2.11. **Step 11.** Check column-beam relationship limitations according to Section 5.4 *(AISC 358, 2010)*

There are also geometric limitations to RWS connection which have been tabulated in Table 18, and they show the limits of geometric parameters tested within this parametric study.

Table 18. Parametric limitations on prequalification.

Parameter	**Minimum** (mm)	**Maximum** (mm)
t_f	8.5	19.0
b_f	100	263
d	200	753
d_0/d	0.65	0.8
S/d	0.6	1.4
Span/d	7	40
t_f = thickness of beam flange, mm b_f = width of beam flange, mm d = depth of connecting beam, mm d_0/d = opening height to beam depth ratio. S/d = opening distance to beam depth ratio. Span/d = beam's span over beam's depth ratio.		

V_{RWS} Computation:

Step 4 of the design procedure requires computation of the shear force at the centre of the RWS cut. This shear force is a function of the gravity load on the beam and the plastic moment capacity of the RWS. An example calculation is shown in **Figure 18** for the case of a beam with a uniformly distributed gravity load. For gravity load conditions other than a uniform load, the appropriate adjustment should be made to the free-body diagram in **Figure 18** and to V_{RWS} and V'_{RWS} Equations.

$$V_{RWS} = \frac{2M_{pr}}{L_h} + \frac{wL_h}{2} \qquad V'_{RWS} = \frac{2M_{pr}}{L_h} - \frac{wL_h}{2}$$

7. Discussion and concluding remarks

Perforated beams' moment capacity is decreased in comparison with the solid-webbed beams. In most cases, by increasing the web opening depth, d_0, and decreasing the web opening end distance, S, moment capacity decreases, thus opening depth, d_0, has a high impact on the beam's moment capacity. However, as the opening size increases, its impact on strength degradation of beam-to-column connections becomes less severe in the final cycles of loading protocol, when such perforated beams are used. At the same time, the introduction of web openings increases the ductility of the connections. Larger openings demonstrate high inelastic deformation with each successive cyclic load. The dissipated energy is influenced by both the moment capacity and ultimate rotational capacity of the

connection. The onset of local web buckling in the vicinity of the web opening is followed by strength degradation. Local web buckling is mainly observed in connections with small web openings; in connections with larger opening sizes a combination of failure modes is taking place, at first the Vierendeel mechanism starts to propagate in the vicinity of the web opening followed by local web buckling happens.

High-stress concentration in the vicinity of the web opening may even lead to steel fracture according to the literature. When large openings are used, such stresses are more concentrated and develop the so-called Vierendeel plastic hinges (four of them fully formed around the edge of an opening across the entire web depth). Oppositely, when smaller opening sizes are used and positioned near the column face, the Vierendeel plastic hinges are not fully developed while high stresses may appear near the column face and the critical zones of the connection (i.e., welding area and column shear panel).

With regards to the effect of the end distance of the openings from the column face, typically increasing the opening distance takes the stress away from column face as long as the openings are large enough to reduce the capacity of the beams. It is worth to note that for different opening sizes the effect of the end distance is varied and in certain cases, no beneficial behaviour is observed – for example when small a web opening appears far from the column face, there is no 'RWS effect'. For all specimens with any opening category (shape and size) or span, increasing the distance from the column face will increase the moment capacity of the connection along with the shear capacity of the beam.

When larger section sizes are used, the stress and strain patterns look similar, thus it is concluded that the plastic hinge pattern is dependent on the opening size and position as well as beam span but not the section size per se. Long span beams start yielding at around cycle 26 with a peak deformation of 0.03rad while short span beams start yielding starts at around cycle 18 with a peak deformation of 0.01rad.

Imperfections were not considered in this study as it has been proven in the literature that they will not affect the results significantly, in comparison to other geometric parameters, such as the web-post width (distance between openings) and the thickness of the web. This limitation is worth to be investigated in future studies, thus GMNIA FE analyses are required to obtain more accurate results followed by experimental validations of the exact models. However, it is expected that when the same imperfection will be applied globally to all the comparative models, the results and conclusions will be the same.

In conclusion, the positive effect on RWS connections on deep column-to-beam connections using European profiles has been demonstrated with the geometric effect of certain geometric parameters to define the trend of the results.

8. Appendix

Table 15 specimens' results have been tabulated in **Table 19**.

Table 19. New test specimens' results.

Specimen	Span /h	d_0 (mm)	M_y (kNm)	M_u (kNm)	θ_y (rad)	θ_u (rad)	D_θ	K_i (kNm/rad)	WOA (cm^2)	E (kNm.rad)	M_{yEC} (kNm)	M_{yR}	CFS	PHS
F-solid-1.6	8.0	0	66.8	110.4	0.0082	0.0587	7.15	9624	0	59.3	67.4	1.00	VH	CF
F2-185-1.6	8.0	130	56.4	72.6	0.0085	0.0595	7.00	8491	133	47.7	56.9	0.84	H	F
F2-185-6	30.0	130	61.3	84.0	0.0180	0.0525	2.92	3604	133	34.5	61.8	0.92	H	P
F2-345-1.6	8.0	130	59.3	83.0	0.0084	0.0594	7.07	8566	133	47.8	59.8	0.89	H	F
F2-345-6	30.0	130	64.6	84.9	0.0191	0.0511	2.68	3607	133	34.1	65.2	0.97	H	P
F3-200-1.6	8.0	160	37.1	48.9	0.0064	0.0596	9.31	6447	201	32.8	37.5	0.56	L	F
F3-200-6	30.0	160	53.8	62.0	0.0154	0.0524	3.40	3550	201	26.9	54.2	0.80	L	F
F3-360-1.6	8.0	160	40.7	53.8	0.0072	0.0593	8.23	6533	201	36.2	41.0	0.61	L	F
F3-360-6	30.0	160	59.4	65.2	0.0185	0.0524	2.83	3556	201	27.6	59.9	0.89	L	F
G-solid-1.9	8.0	0	107.4	160.6	0.0074	0.0582	7.87	15003	0	80.9	111.9	1.00	VH	CF
G2-222-1.9	8.0	156	87.6	114.7	0.0078	0.0580	7.43	13302	191	71.8	91.3	0.82	M	F
G2-222-7.2	30.0	156	100.7	129.3	0.0179	0.0521	2.91	5840	191	53.9	104.9	0.94	M	F
G2-414-1.9	8.0	156	89.1	130.7	0.0075	0.0580	7.73	13407	191	69.2	92.8	0.83	M	F
G2-414-7.2	30.0	156	103.3	133.0	0.0179	0.0519	2.90	5845	191	55.0	107.7	0.96	H	P
G3-240-1.9	8.0	192	59.8	78.4	0.0065	0.0578	8.89	10256	290	50.8	62.3	0.56	L	F
G3-240-7.2	30.0	192	92.5	101.2	0.0168	0.0518	3.08	5755	290	43.3	96.4	0.86	L	F
G3-432-1.9	8.0	192	64.6	85.9	0.0073	0.0580	7.95	10388	290	55.7	67.3	0.60	L	F
G3-432-7.2	30.0	192	97.9	106.7	0.0183	0.0520	2.84	5766	290	45.8	102.0	0.91	L	F
H-solid-2.2	8.0	0	137.6	206.5	0.0072	0.0573	7.96	19546	0	101.1	147.6	1.00	VH	CF
H2-250-2.2	8.0	175.5	115.4	150.7	0.0078	0.0571	7.32	17353	242	90.5	123.8	0.84	M	F
H2-250-8.1	30.0	175.5	132.6	162.4	0.0178	0.0511	2.87	7682	242	66.7	142.2	0.96	M	F
H2-466-2.2	8.0	175.5	116.1	171.6	0.0074	0.0556	7.52	17477	242	89.8	124.5	0.84	M	F
H2-466-8.1	30.0	175.5	134.9	172.0	0.0178	0.0520	2.92	7690	242	71.0	144.7	0.98	H	P
H3-270-2.2	8.0	216	73.8	102.6	0.0058	0.0568	9.80	13510	366	65.7	79.2	0.54	L	F
H3-270-8.1	30.0	216	120.0	131.5	0.0162	0.0513	3.17	7571	366	54.8	128.7	0.87	L	F
H3-486-2.2	8.0	216	81.7	111.8	0.0068	0.0571	8.40	13663	366	70.3	87.7	0.59	L	F
H3-486-8.1	30.0	216	129.3	138.5	0.0181	0.0512	2.83	7587	366	56.4	138.7	0.94	L	F
I-solid-6	8.0	0	1465.5	2117.9	0.0065	0.0567	8.72	236366	0	935.2	1483.8	1.00	VH	CF
I2-694-6	8.0	487.5	1215.6	1590.5	0.0060	0.0565	9.41	212073	1867	607.7	1230.8	0.83	M	F
I2-694-22.5	30.0	487.5	1310.9	1587.2	0.0162	0.0517	3.19	82170	1867	606.4	1327.3	0.89	M	F
I2-1294-6	8.0	487.5	1245.4	1815.9	0.0060	0.0564	9.39	214242	1867	673.5	1261.0	0.85	M	F
I2-1294-22.5	30.0	487.5	1401.6	1630.7	0.0177	0.0515	2.91	82273	1867	633.9	1419.1	0.96	M	F
I3-750-6	8.0	600	875.6	1112.6	0.0056	0.0448	8.00	165486	2827	526.5	886.5	0.60	L	F
I3-750-22.5	30.0	600	1187.0	1299.0	0.0150	0.0517	3.45	80735	2827	505.5	1201.8	0.81	L	F
I3-1350-6	8.0	600	906.9	1243.6	0.0056	0.0566	10.1	169469	2827	506.8	918.2	0.62	L	F
I3-1350-22.5	30.0	600	1215.3	1359.6	0.0151	0.0517	3.43	80960	2827	486.0	1230.5	0.83	L	F

Table 20. All test setup results raw data.

Specimen	Span /h	d_0 (mm)	M_y (kNm)	M_u (kNm)	θ_y (rad)	θ_u (rad)	D_θ	K_i (kNm/rad)	WOA (cm^2)	E (kNm.rad)	M_{yEC} (kNm)	M_{yR}	CFS	PHS
B-Solid-3	9.1	0	245.3	330.8	0.0103	0.0551	5.35	27306	0	149.0	245.2	1	VH	CF
B1-287-3	9.1	165	234.9	293.7	0.0102	0.0549	5.38	26848	214	138.0	238.8	0.97	M	F
B1-287-15	45.5	165	230.3	273.4	0.0278	0.0509	1.83	8595	214	111.6	230.3	0.94	M	O
B1-574-3	9.1	165	244.6	315.8	0.0107	0.0549	5.13	26921	214	152.0	247.7	1.01	VH	CF
B1-574-15	45.5	165	236.2	269.9	0.0306	0.051	1.67	8598	214	92.5	242.4	0.99	H	CF
B2-287-3	9.1	214.5	211.7	251.2	0.01	0.054	5.4	25618	361	122.9	215.3	0.88	M	F
B2-287-15	45.5	214.5	218.6	270.7	0.0278	0.0501	1.8	8564	361	88.6	220.8	0.9	M	O
B2-574-3	9.1	214.5	231.8	292.2	0.0109	0.0552	5.06	25793	361	121.0	235.3	0.96	L	F
B2-574-15	45.5	214.5	228.2	271.8	0.0278	0.0504	1.81	8569	361	90.0	228.1	0.93	M	O
B3-287-3	9.1	264	127.7	175.5	0.0106	0.0552	5.21	21915	547	96.5	163.3	0.67	L	F
B3-287-15	45.5	264	204.9	219.2	0.0278	0.0509	1.83	8491	547	76.9	204.8	0.84	L	F
B3-574-3	9.1	264	139.5	192.2	0.0106	0.0552	5.21	22264	547	105.1	173.7	0.71	L	F
B3-574-15	45.5	264	212.5	227.4	0.0278	0.051	1.83	8505	547	79.0	212.5	0.87	L	F
C-Solid-3	6.7	0	580.1	856.0	0.0107	0.0573	5.36	75426	0	453.8	519.1	1	VH	CF
C1-392-3	6.7	225	535.1	655.3	0.0112	0.0559	5	70988	398	303.9	478.8	0.92	M	F
C1-392-15	33.3	225	497.3	635.4	0.0223	0.0507	2.27	24803	398	238.2	445.0	0.86	M	O
C1-783-3	6.7	225	562.4	737.1	0.0111	0.0578	5.2	71253	398	322.6	503.2	0.97	L	F
C1-783-15	33.3	225	507.9	636.1	0.0219	0.0493	2.25	24807	398	236.0	454.5	0.88	M	O
C2-392-3	6.7	292.5	462.9	519.0	0.0103	0.0566	5.49	64202	672	236.2	414.2	0.8	L	F
C2-392-15	33.3	292.5	466.4	627.4	0.0205	0.0512	2.5	24654	672	237.1	417.4	0.8	M	P
C2-783-3	6.7	292.5	511.7	603.8	0.0111	0.0572	5.15	65049	672	257.4	457.8	0.88	L	F
C2-783-15	33.3	292.5	497.8	630.6	0.0223	0.0497	2.23	24676	672	238.8	445.5	0.86	M	P
C3-392-3	6.7	360	309.4	330.3	0.0114	0.0576	5.05	44376	1018	219.5	276.8	0.53	L	F
C3-392-15	33.3	360	423.0	460.5	0.0187	0.0516	2.76	24310	1018	187.7	378.5	0.73	L	F
C3-783-3	6.7	360	327.0	362.3	0.0112	0.0573	5.12	45171	1018	247.1	292.6	0.56	L	F
C3-783-15	33.3	360	447.5	483.8	0.0206	0.0511	2.48	24364	1018	193.3	400.5	0.77	L	F
D-Solid-5	10.0	0	698.3	1098.9	0.0108	0.0549	5.08	82854	0	529.4	669.2	1	VH	CF
D1-435-5	10.0	250	668.6	847.9	0.0102	0.0551	5.41	80731	491	427.7	640.7	0.96	M	F
D1-435-20	40.0	250	642.7	785.9	0.0264	0.0512	1.94	27487	491	273.2	615.9	0.92	M	O
D1-870-5	10.0	250	695.8	1030.7	0.0108	0.055	5.09	80926	491	488.1	666.8	1	M	F
D1-870-20	40.0	250	667.6	790.6	0.0279	0.0512	1.83	27496	491	277.8	639.8	0.96	M	O
D2-435-5	10.0	325	600.4	730.6	0.0107	0.0548	5.12	69359	830	376.9	575.4	0.86	L	F
D2-435-20	40.0	325	600.7	745.8	0.0233	0.0511	2.19	27351	830	271.6	575.7	0.86	M	P
D2-870-5	10.0	325	683.4	835.5	0.0108	0.0544	5.04	78001	830	368.8	654.9	0.98	L	F
D2-870-20	40.0	325	634.5	779.7	0.0264	0.0508	1.92	27373	830	275.6	608.0	0.91	M	P
D3-435-5	10.0	400	496.6	526.6	0.0109	0.0538	4.94	67869	1257	304.7	475.9	0.71	L	F
D3-435-20	40.0	400	555.1	602.3	0.0241	0.0513	2.13	27042	1257	228.4	531.9	0.79	L	F
D3-870-5	10.0	400	535.7	578.6	0.0109	0.0553	5.07	69058	1257	333.8	513.3	0.77	L	F
D3-870-20	40.0	400	577.4	629.9	0.0241	0.0512	2.12	27090	1257	235.6	553.4	0.83	L	F
E-Solid-5	8.3	0	1181.1	1561.3	0.0111	0.0566	5.1	150294	0	820.2	1071.2	1	VH	CF
E1-522-5	8.3	300	1111.5	1367.4	0.0111	0.0567	5.1	144969	707	641.6	1008.0	0.94	M	F
E1-522-20	33.3	300	974.8	1097.9	0.024	0.0516	2.15	45069	707	431.1	884.0	0.83	M	F
E1-1044-5	8.3	300	1164.3	1538.3	0.0111	0.056	5.05	145189	707	715.2	1056.0	0.99	L	F
E1-1044-20	33.3	300	1002.9	1151.0	0.0239	0.0517	2.16	45246	707	444.5	909.5	0.85	M	P
E2-522-5	8.3	390	1009.0	1171.8	0.0111	0.0567	5.1	136538	1195	545.1	915.1	0.85	L	F
E2-522-20	33.3	390	920.0	1206.5	0.0221	0.0494	2.23	44948	1195	441.4	834.4	0.78	M	P
E2-1044-5	8.3	390	1124.8	1290.3	0.0111	0.0562	5.07	137652	1195	546.1	1020.1	0.95	L	F
E2-1044-20	33.3	390	959.1	1179.9	0.0233	0.0515	2.21	44738	1195	445.9	869.8	0.81	M	P
E3-522-5	8.3	480	759.3	797.0	0.011	0.0564	5.13	110000	1810	480.5	688.6	0.64	L	F
E3-522-20	33.3	480	828.4	906.2	0.0207	0.0516	2.49	44313	1810	364.9	751.3	0.7	L	F
E3-1044-5	8.3	480	822.0	882.9	0.0112	0.0488	4.36	112282	1810	509.2	745.5	0.7	L	F
E3-1044-20	33.3	480	883.3	941.8	0.023	0.0513	2.23	44175	1810	363.6	801.1	0.75	L	F

References

ABAQUS, 2014. *Users manual 6.14.* Providence, RI, USA: Dassault Systèmes Simulia Corp.

AISC 341, 2010. *Seismic Provisions for Structural Steel Buildings.* Chicago: American Institute Of Steel Construction.

AISC 358, 2010. *Prequalified Connections for Special and Intermediate Steel Moment Frames for Seismic Applications, 358-10.* Chicago: American Institute Of Steel Construction.

AISC 360, 2010. *Specification for Structural Steel Buildings, AISC/ANSI 360-10.* Chicago: American Institute of Steel Construction.

EC8. Part 3, 2005. *Design of Structures for Earthquake Resistance. Assessment and Retrofitting of Buildings EN 1998-3.* Brussels, Belgium: EN.

Erfani, S. & Akrami, V., 2017. Increasing Seismic Energy Dissipation of Steel Moment Frames Using Reduced Web Section (RWS) Connection. *Journal of Earthquake Engineering,* 21(7), pp. 1090-1112.

Eurocode 3, 2005. *Design of Steel Structures – Part1: General Rules and Rules for Buildings EN 1993-1-1.* Brussels, Belgium.: EN.

FEMA 350, 2000. *Recommended Seismic Design Criteria for the New Steel Moment Frame Buildings, Report No. FEMA 350.* CA: SAC Joint Venture.

Hedayat, A.A. and Celikag, M., 2009. Post-Northridge connection with modified beam end configuration to enhance strength and ductility. J*ournal of Constructional Steel Research*, 65, pp. 1413-1430.

Kiani, J. & Tsavdaridis, K. D., 2018. Seismic Assessment of Reduced Web Section (RWS) and Reduced Beam Section (RBS) Steel Frames: A Comparative Study. *Soil Dynamics and Earthquake Engineering; Special Issue on Advances in Seismic Design and Assessment of Steel Structures.*

Li, R., Yu, Y., Samali, B. & Li, C., 2019. Parametric Analysis on the Circular CFST Column and RBS Steel Beam Joints. *Materials,* 12(9), p. 1535.

Momenzadeh, S., Kazemi, M. T. & Asl , M. H., 2017. Seismic performance of reduced web section moment connections. *International Journal of Steel Structures,* 17(2), pp. 413-425.

Nascimbene, R., 2014. Towards Non–Standard Numerical Modeling of Thin-Shell Structures: Geometrically Linear Formulation. *International Journal for Computational Methods in Engineering Science and Mechanics,* 15(2), pp. 126-141.

Naughton, D. T., Tsavdaridis, K.D., Maraveas, C. & Nicolaou, A., 2017. Pushover analysis of steel seismic resistant Frames with reduced Web section and reduced Beam section connections. *Frontiers in Built Environment,* Volume 3, p. 59.

Naughton, D. T., Tsavdaridis, K. D., Maraveas, C. & Nicolaou, A., 2017. Pushover Analysis of Steel Seismic Resistant Frames with RWS and RBS Connections. *Frontiers in Built Environment,* 3(59).

Pachoumis, D. T., Galoussis E. G., Kalfas C. N. & Christitsas A.D., 2009. Reduced beam section moment connections subjected to cyclic loading: Experimental analysis and FEM simulation. *Engineering Structures,* 31(1), pp. 216-223.

SAC, 2000. *Seismic design criteria for new moment-resisting steel frame construction. Report no. FEMA 350.* Sacramento, CA: SAC Joint Venture.

Shaheen, M. A., Tsavdaridis, K. D. & Yamada, S., 2018. Comprehensive FE Study of the Hysteretic Behavior of Steel–Concrete Composite and Noncomposite RWS Beam-to-Column Connections. *Journal of Structural Engineering,* 144(9).

Sophianopoulos, D. S. & Deri, A. E., 2017. Steel beam-to-column RBS connections with European profiles: I. Static optimization. *Journal of Constructional Steel Research,* Volume 139, pp. 101-109.

Tsavdaridis, K.D., 2014. Strengthening techniques: code-deficient steel buildings. *Encyclopedia of Earthquake Engineering, Springer Berlin Heidelberg,* pp. 1-26.

Tsavdaridis, K. D. & D'Mello, C., 2011. Finite element investigation on web-post buckling of perforated steel beams with various web opening shapes subjected under different shear-moment. *EUROSTEEL,* Volume C, pp. 1851-1856.

Tsavdaridis, K. D. & D'Mello, C., 2012. Vierendeel bending study of perforated steel beams with various novel web opening shapes through nonlinear finite-element analyses.. *Journal of Structural Engineering,* pp. 1214-1230.

Tsavdaridis, K. D., Faghih, F. & Nikitas, N., 2014. Assessment of perforated steel beam-to-column connections subjected to cyclic loading. *Journal of Earthquake Engineering,* 18(8), pp. 1302-1325.

Tsavdaridis, K. D., Pilbin, C. & Lau, C. K., 2017. FE Parametric Study of RWS/WUF-B Moment Connections with Elliptically-Based Beam Web Openings under Monotonic and Cyclic Loading. *International Journal of Steel Structures,* Volume 17, pp. 677-694.

Uang, C. M., Yu, Q. K., Noel, S. & Gross, J., 2000. Cyclic testing of steel moment connections rehabilitated with RBS or welded haunch. *Journal of Structural Engineering,* 126(1), pp. 57-68.

Uang, C. M., Yu, Q. S. & Gilton, C. S., 2000b. Effects of loading history on cyclic performance of steel RBS moment connections. *Proceedings of the 12th WCEE, Upper Hutt, New Zealand.*

Wang, W. D., Han, L. H. & Uy, B., 2008. Experimental behaviour of steel reduced beam section to concrete-filled circular hollow section column connections. *Journal of Constructional Steel Research,* 64(5), pp. 493-504.

Yang, Q., Li, B. & Yang, N., 2009. Aseismic behaviors of steel moment resisting frames with opening in beam web. *Journal of Constructional Steel Research,* 65(6), pp. 1323-1336.

FIGURES next 18 pages…

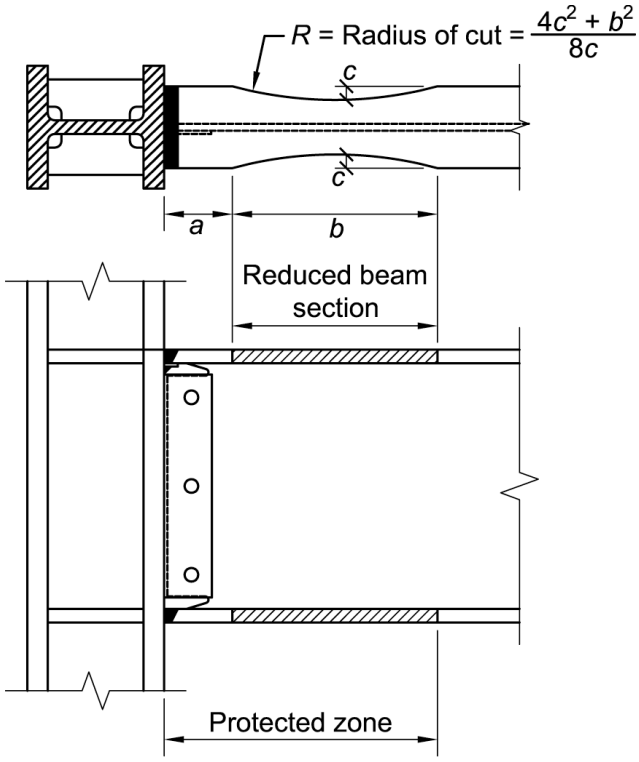

Figure 1. Reduced beam section connection (RBS). (AISC 358, 2010).

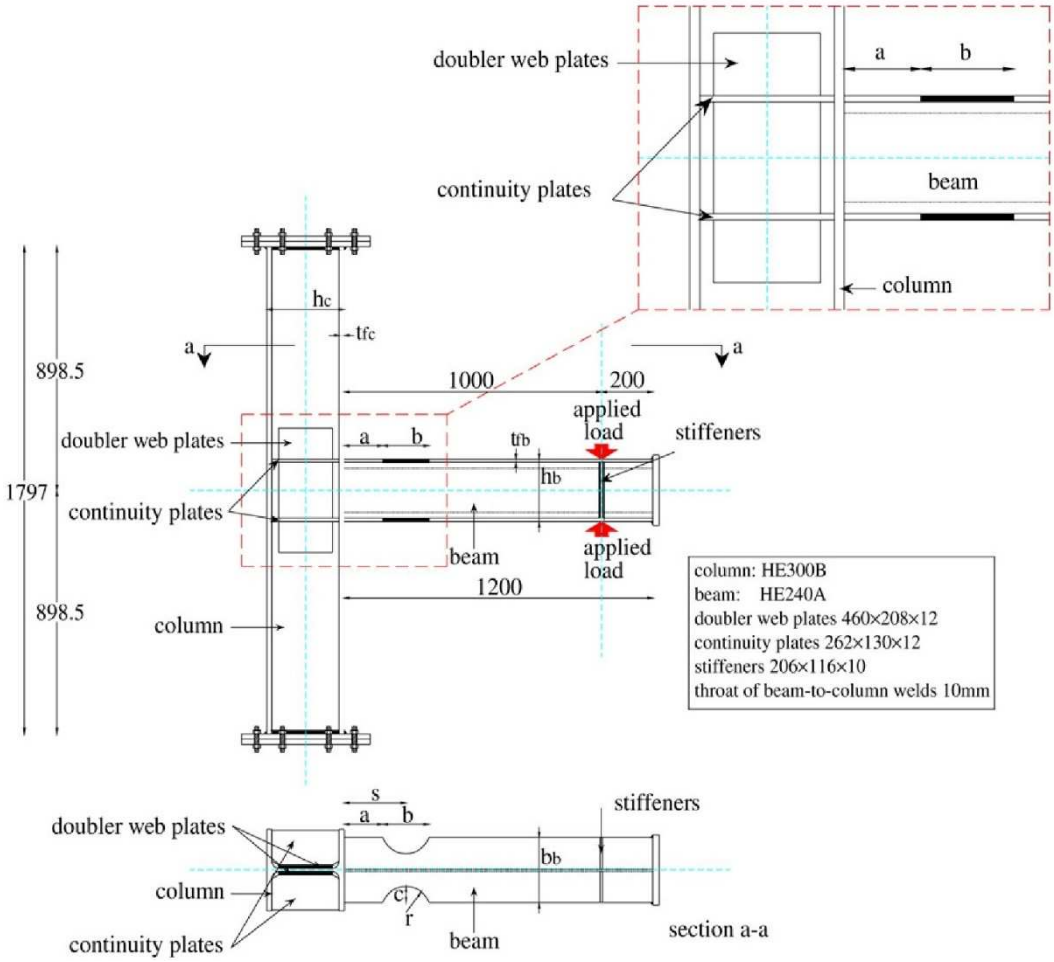

Figure 2. Test set-up (Pachoumis, et al., 2009)

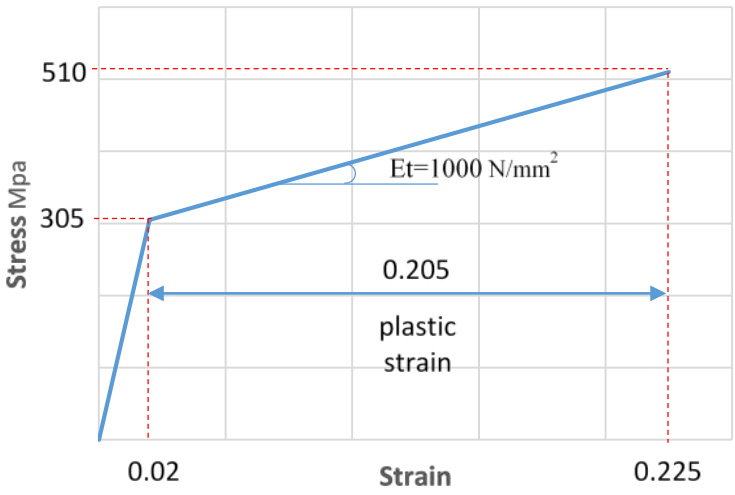

Figure 3. Material stress-stain curve

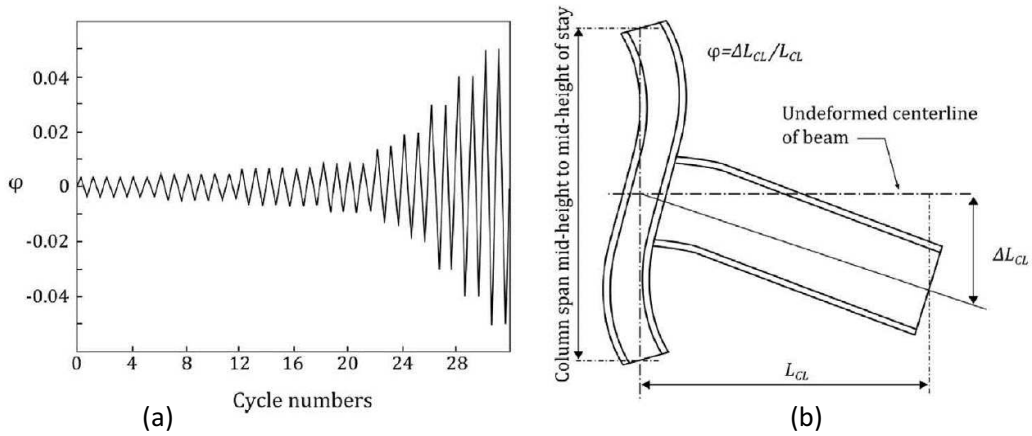

Figure 4. SAC loading protocol: (a) Loading sequence; (b) Angular rotation of test assembly (FEMA 350,

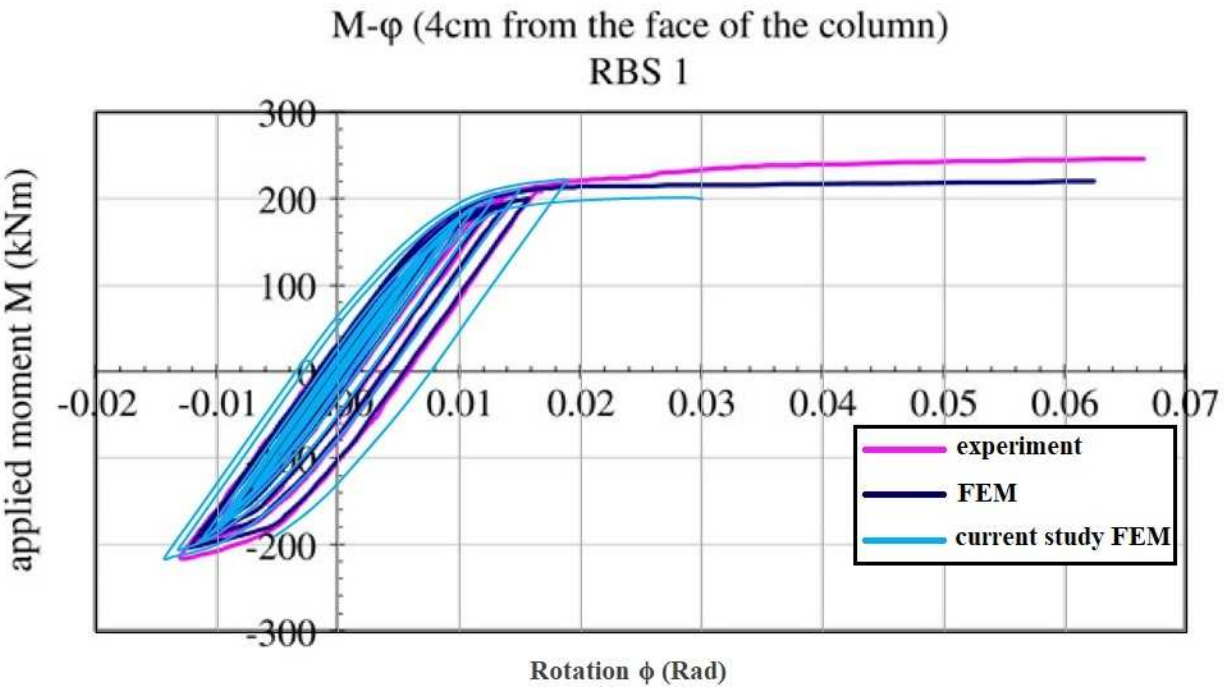

Figure 5. Moment Rotation Curve, 4cm away from column face (Pachoumis, et al., 2009).

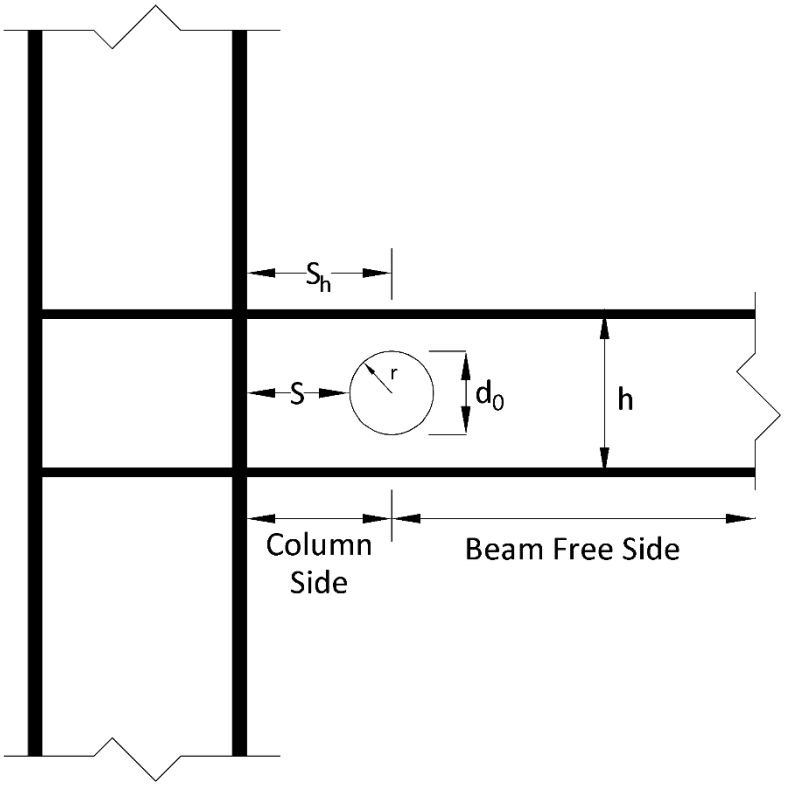

d_0: 0.50h, 0.65h, 0.80h
S: 0.60h, 1.00h, 1.40h

Where h is the total beam height which depends on the test setup.

Figure 6. RWS parameters.

d_0 Diameter of circular web opening, web opening height
S_h Opening distance from opening centre to column face

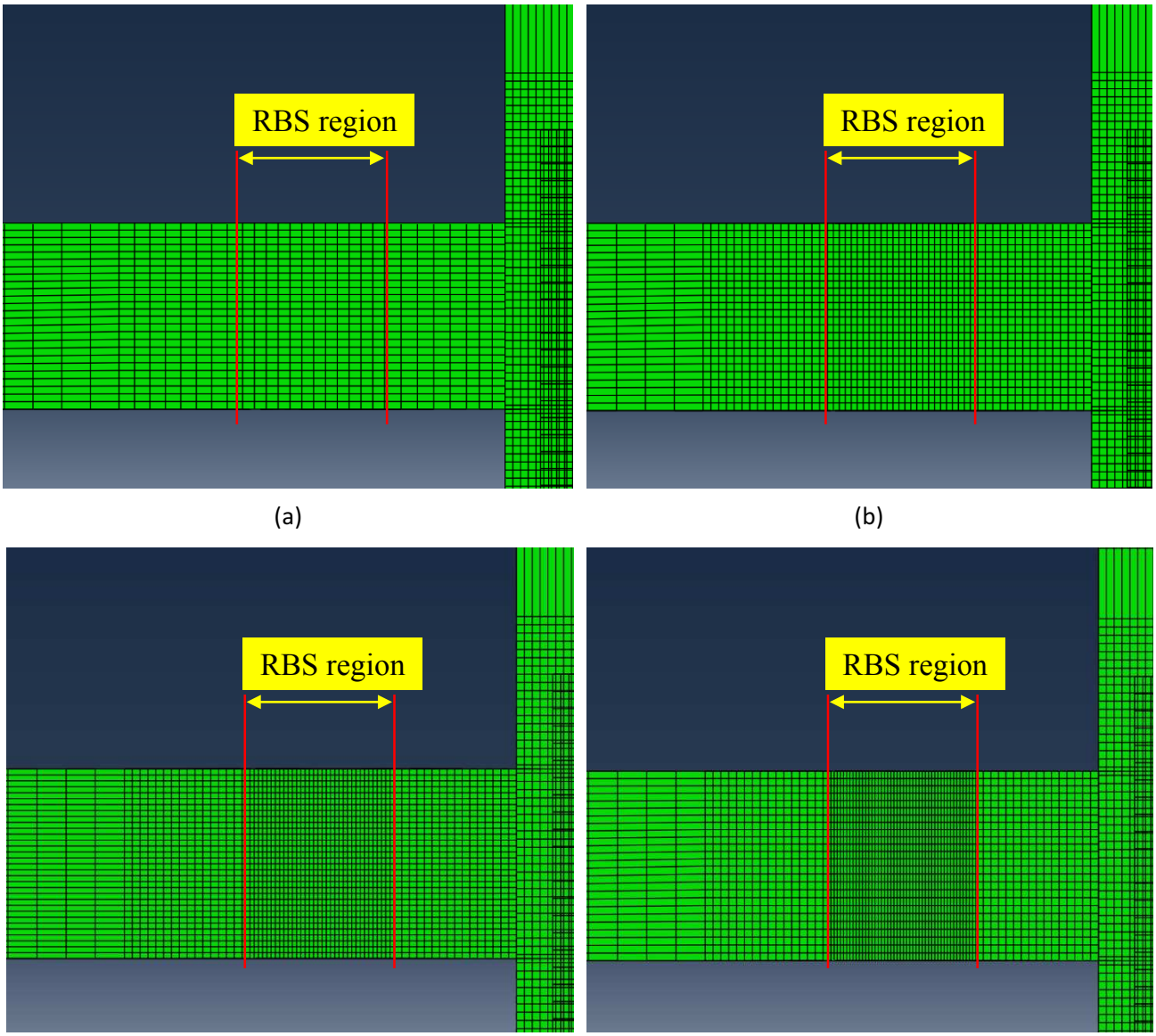

Figure 7. Mesh Study: (a) Coarse; (b) Medium; (c) Fine; (d) Very Fine

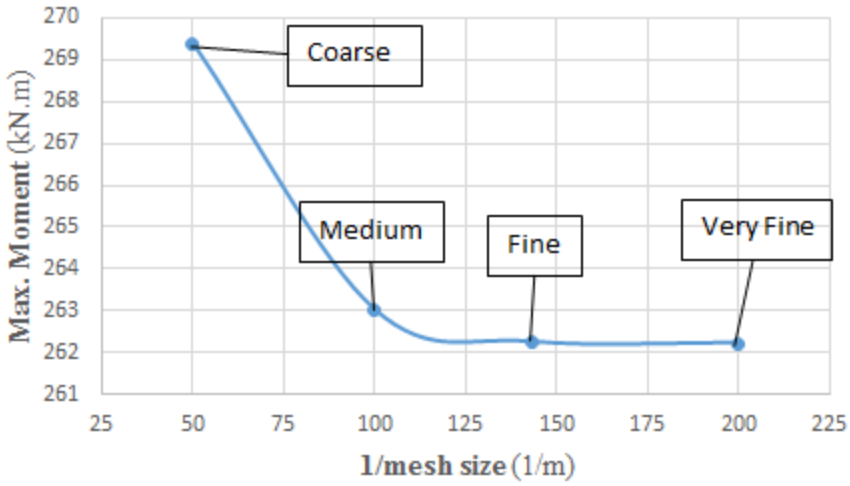

Figure 8. Mesh results

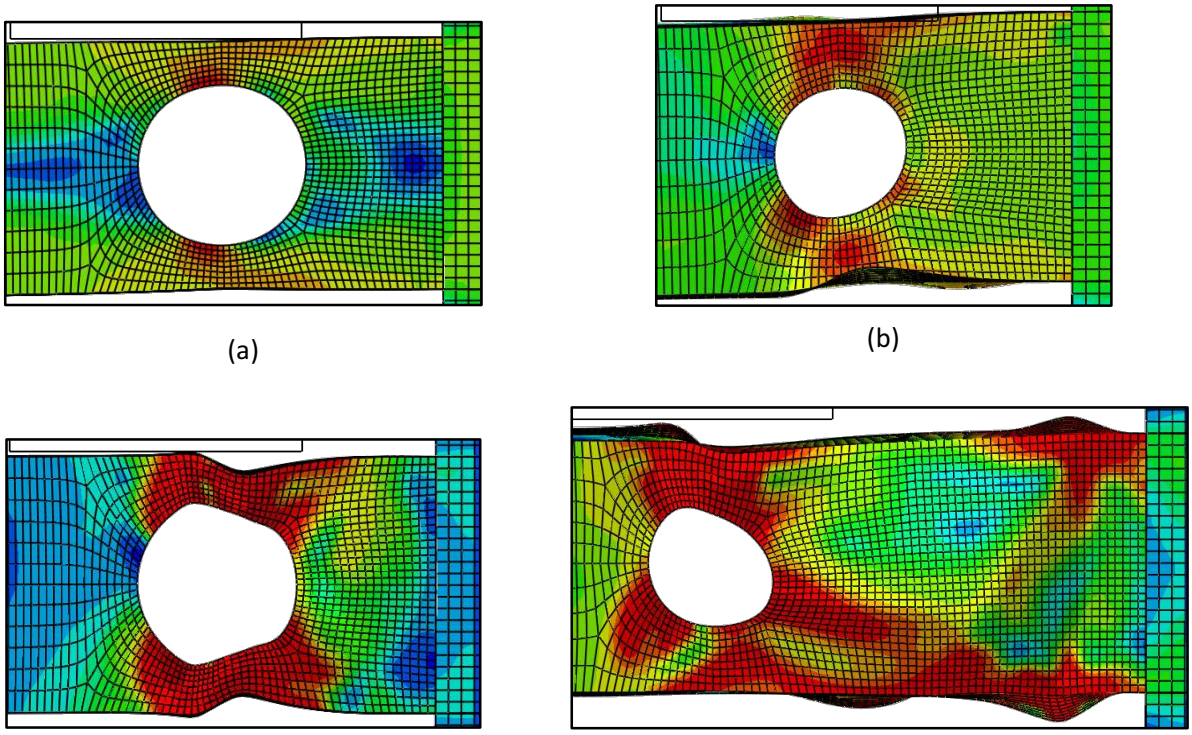

Figure 9. Plastic Hinge Formation types: (a) Opening; (b) Partial; (c) Full; (d) Column Face

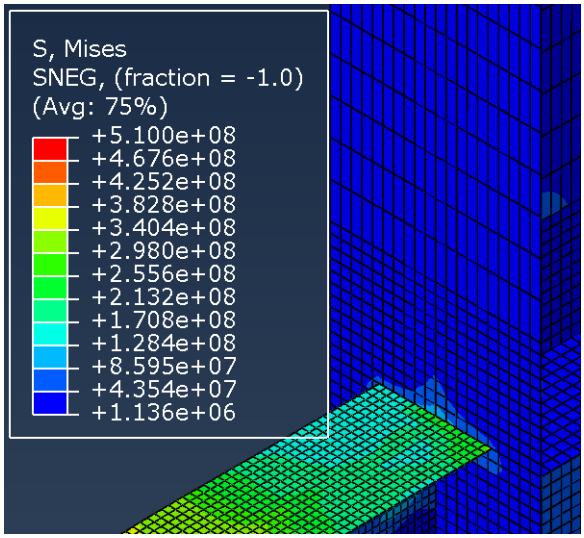

(a)

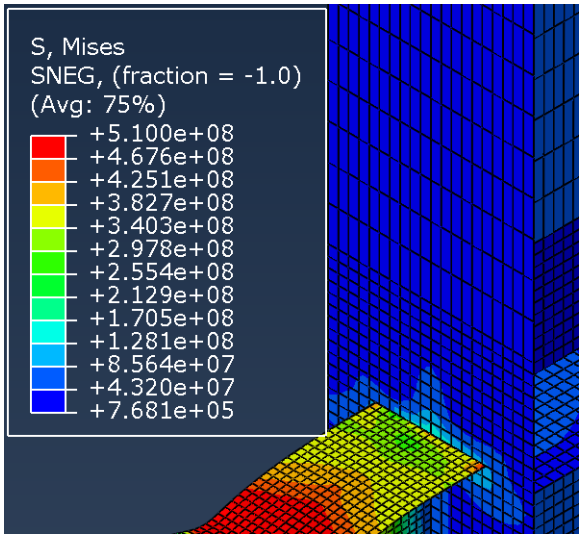

(b)

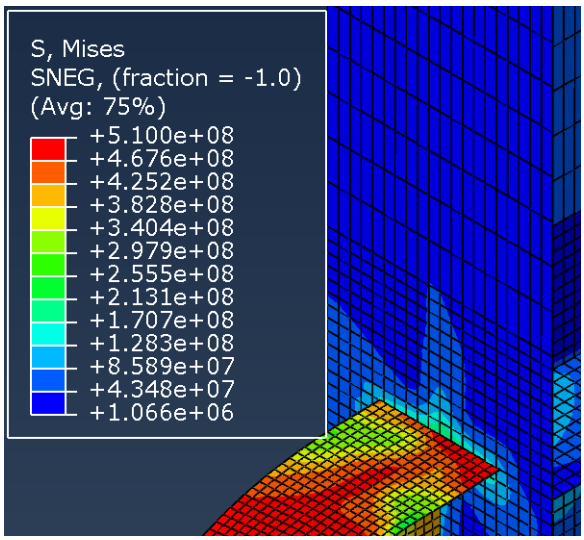

(c)

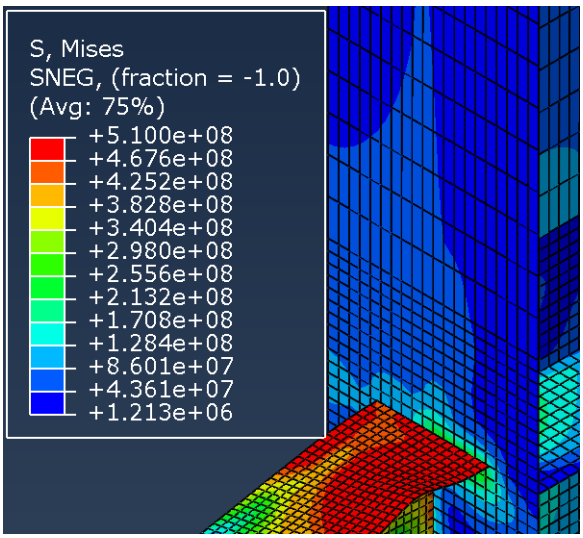

(d)

Figure 10. Column Face Stress: (a) Low; (b) Moderate; (c) High; (d) Very High

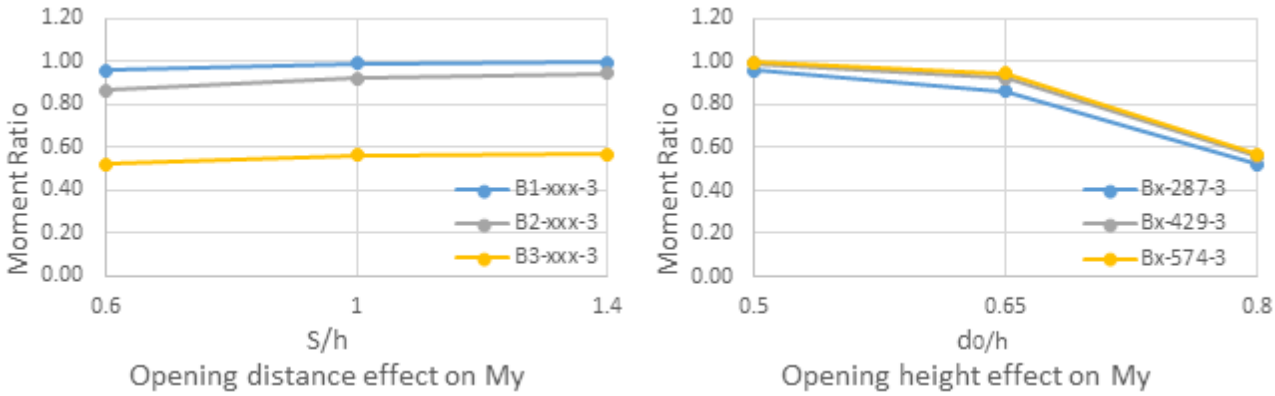

Figure 11. Effect on yield moment (also similar for Mu) of: (a) Opening distance and (b) height

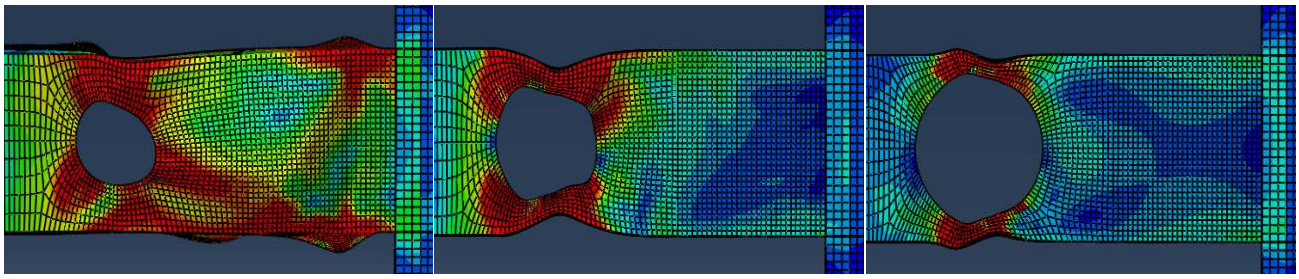

(a) (b) (c)

Figure 12. Representative opening size effect on Column Face Stress: (a) d_0=0.50h; (b) d_0=0.65h; (c) d_0=0.80h

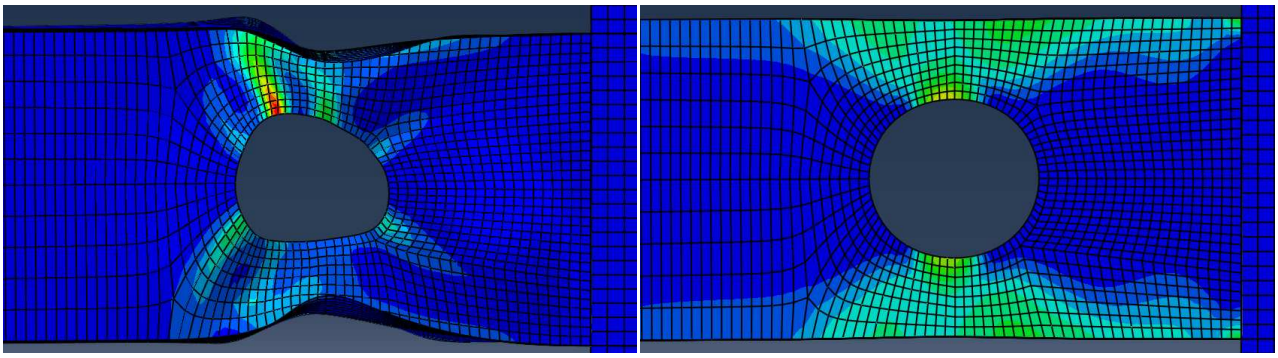

(a) (b)

Figure 13. Representative equivalent plastic strain of any span/depth ratio, Beam span effect on PHF: (a) 3m; (b) 15m

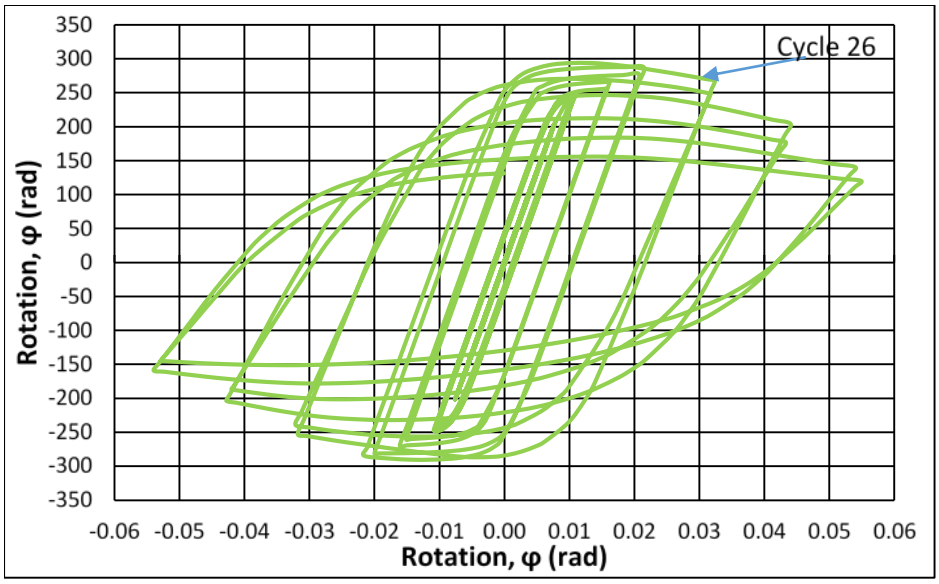

Figure 14. Web buckling triggering strength degradation (d_0=0.5h)

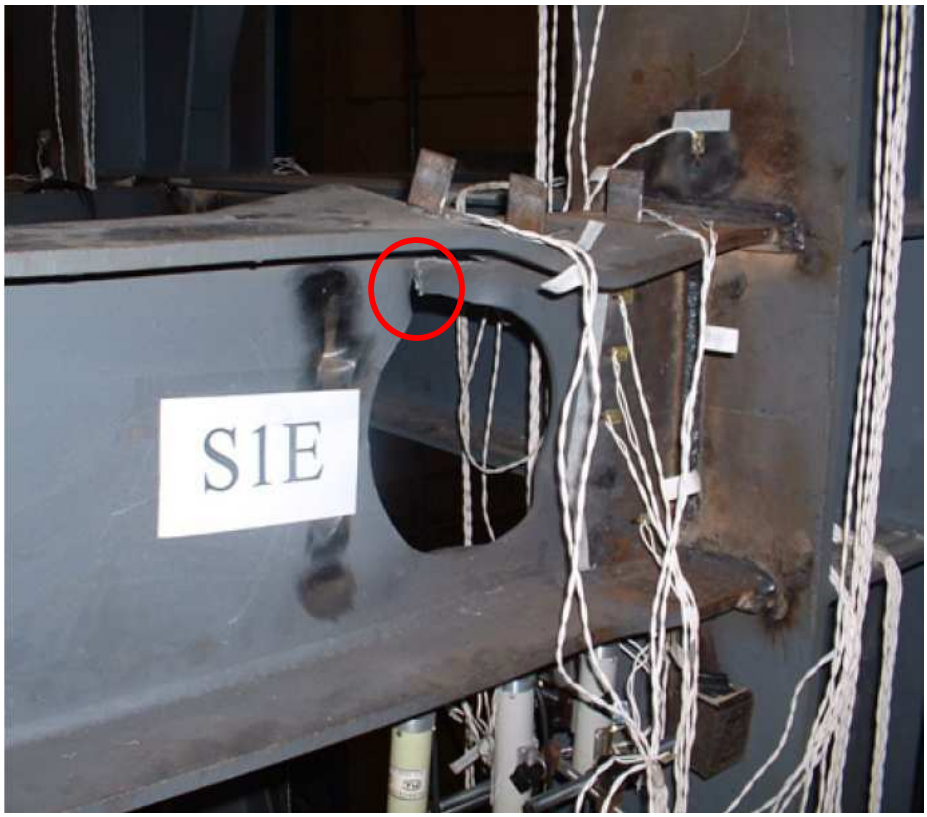

Figure 15. Failure mode of connection with web opening (Yang, et al., 2009)

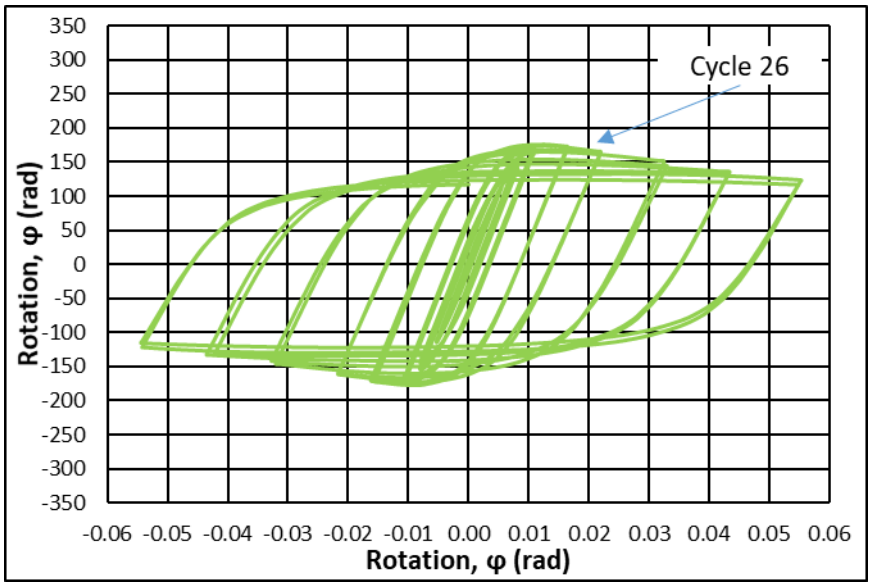

Figure 16. Vierendeel mechanism triggering degradation (d_0=0.8h)

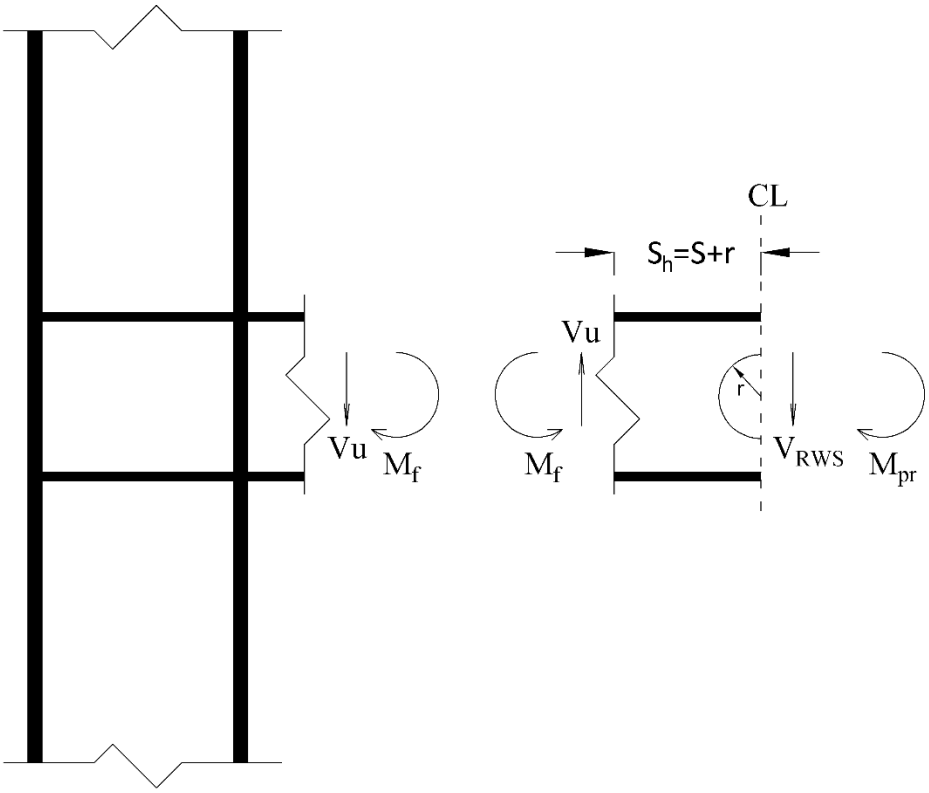

Figure 17. Free-body diagram between centre of RWS and face of column.

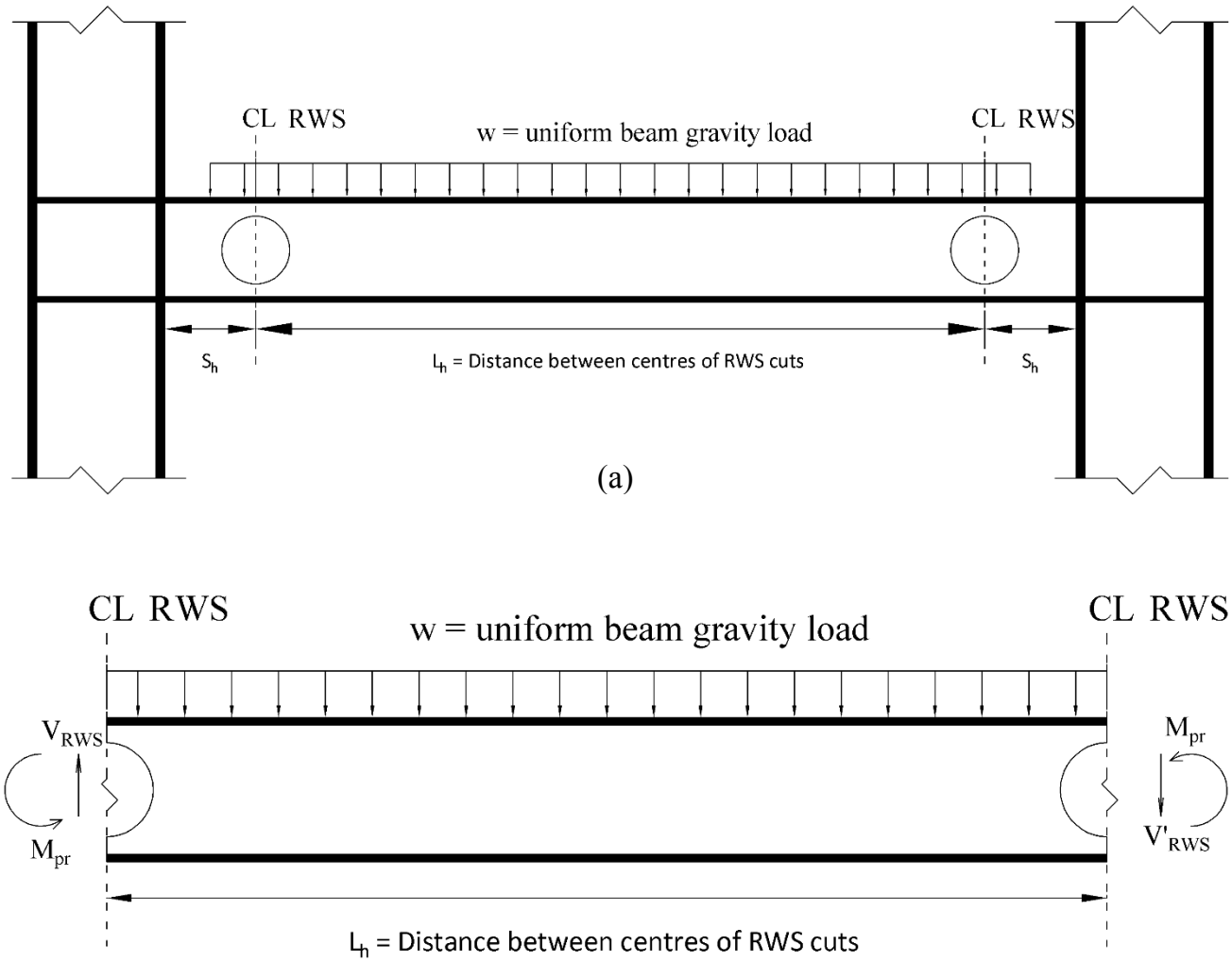

Figure 18. Example calculation of shear at centre of RWS cuts. (AISC 358, 2010)

(a) Beam with RWS cuts and uniform gravity load;

(b) Free-body diagram of beam between RWS cuts and calculation of shear at RWS.